SPATIAL STATISTICS OF INSTRUMENT-LIMITED ANGULAR MEASUREMENT ERRORS IN PHASED ARRAY RADARS

R. H. Sahmel, et al

Aerospace Corporation

Prepared for:

Air Force Systems Command

2 October 1972

AIR FORCE REPORT NO.
SAMSO-TR-72-309

AEROSPACE REPORT NO.
TR-0073(3901-02)-1

Spatial Statistics of Instrument-Limited Angular Measurement Errors in Phased Array Radars

Prepared by R. H. SAHMEL and R. MANASSE
Electronics and Optics Division

72 OCT 02

Engineering Science Operations
THE AEROSPACE CORPORATION

Prepared for SPACE AND MISSILE SYSTEMS ORGANIZATION
AIR FORCE SYSTEMS COMMAND
LOS ANGELES AIR FORCE STATION
Los Angeles, California

DOCUMENT CONTROL DATA - R & D

(Security classification of title, body of abstract and indexing annotation must be entered when the overall report is classified)

1 ORIGINATING ACTIVITY (Corporate author)
The Aerospace Corporation
El Segundo, California

2a REPORT SECURITY CLASSIFICATION
Unclassified

2b GROUP

3 REPORT TITLE
SPATIAL STATISTICS OF INSTRUMENT-LIMITED ANGULAR MEASUREMENT ERRORS IN PHASED ARRAY RADARS

4 DESCRIPTIVE NOTES (Type of report and inclusive dates)

5 AUTHOR(S) (First name, middle initial, last name)
R. H. Sahmel and R. Manasse

6 REPORT DATE	7a TOTAL NO OF PAGES	7b NO OF REFS
72 OCT 02	63 65	5

8a CONTRACT OR GRANT NO.	9a ORIGINATOR'S REPORT NUMBER(S)
F04701-72-C-0073	TR-0073(3901-02)-1
b PROJECT NO	
c	9b OTHER REPORT NO(S) (Any other numbers that may be assigned this report)
d	SAMSO-TR-72-309

10 DISTRIBUTION STATEMENT
Approved for public release; distribution unlimited

11 SUPPLEMENTARY NOTES	12 SPONSORING MILITARY ACTIVITY
Details of illustrations in this document may be better studied on microfiche.	Space and Missile Systems Organization Air Force Systems Command Los Angeles, California

13 ABSTRACT

The principal contributors to the random component of the instrument limited angular measurement errors in electronically scanned phased array radars are reviewed and formulas are developed for statistical modeling of these error sources. A comprehensive computer program, embodying this analysis, has been developed for determining these array measurement errors and their spatial correlation statistics, in two angle variables. This program includes the effect of finite computation accuracy in the beam steering computer. The error model employed is valid for space-fed and certain types of corporate-fed arrays. This program is used to evaluate the statistical behavior of angular errors for some typical situations of interest. The use of angle, frequency, and phase "dithering" for improving the correlation statistics of these arrays is examined. The phase dithering technique is shown to be at least as effective as angle and frequency dithering and has the virtue of being readily implemented in the beam steering computer.

14 KEY WORDS

Radar Measurement Errors
Radar Tracking Errors
Radar Angle Error Correlation
Phased Array Measurement Errors
Radar Instrumentation Errors

Distribution Statement (Continued)

Abstract (Continued)

Air Force Report No.
SAMSO-TR-72-309

Aerospace Report No.
TR-0073(3901-02)-1

SPATIAL STATISTICS OF INSTRUMENT-LIMITED ANGULAR MEASUREMENT ERRORS IN PHASED ARRAY RADARS

Prepared by

R. H. Sahmel and R. Manasse
Radar and Power Subdivision
Electronics and Optics Division

72 OCT 02

Engineering Science Operations
THE AEROSPACE CORPORATION
El Segundo, California

Prepared for

SPACE AND MISSILE SYSTEMS ORGANIZATION
AIR FORCE SYSTEMS COMMAND
LOS ANGELES AIR FORCE STATION
Los Angeles, California

IC

FOREWORD

This report is published by The Aerospace Corporation, El Segundo, California, under Air Force Contract No. F04701-72-C-0073.

This report, which documents research carried out from May 1971 through July 1972, was submitted for review and approval on 9 November 1972 to Lt Colonel Elliott W. Porter, (DYX).

The authors acknowledge with gratitude the assistance of L. J. Cantafio, Radar and Communications Department, and C. Crummer, Information Processing Division, both of The Aerospace Corporation. We acknowledge helpful discussions with J. Walsh, D. K. Barton and others at the Raytheon Corporation and L. Schwartzman and P. M. Liebman and others at the Sperry Gyroscope Company.

Approved by

J. W. Capps, Director
Radar and Power Subdivision
Electronics and Optics Division
Engineering Science Operations

Publication of this report does not constitute Air Force approval of the report's findings or conclusions. It is published only for the exchange and stimulation of ideas.

ELLIOTT W. PORTER, Lt Colonel, USAF
Executive Officer
Deputy for Technology

CONTENTS

FIGURES

FIGURES (Continued)

TABLE

GLOSSARY

A	aperture area
D	aperture diameter
d_x	column spacing
d_y	row spacing
F	focal length
i, j	element index in rectangular aperture coordinates or general integer variable
k	propagation constant $= 2\pi/\lambda$
m, n	lattice indices
N	number of phase shifter elements
p	integer variable
Q	phase shifter quantization level spacing (radians)
q	phase shifter quantization levels (bits)
$R_u(\Delta u, \Delta v)$	autocorrelation function of ϵ_u
$R_v(\Delta u, \Delta v)$	autocorrelation function of ϵ_v
R	aperture radius
r	row and column adder quantization level (bits)
s	beam steering computer quantization level (bits)
$\underline{U}$	error function lattice vector
u	$\sin \alpha$

u_o	limit of scan along u
Δu	differential steering angle in sin α
$\underline{V}$	error function lattice vector
Δv	differential steering angle in sin β
v	$\sin\beta$
v_o	limit of scan along v
$\underline{w}$	displacement vector in (u, v) space
x	horizontal aperture coordinate
x_{mn}	x evaluated at mnth lattice point
y	vertical aperture coordinate
y_{mn}	y evaluated at mnth lattice point
α	scan angle off normal toward x
β	scan angle off normal toward y
γ_i	ith bit state function
Δ	difference operator
$\delta_x(x, y)$	x difference pattern amplitude weighting (illumination) function
$\delta_y(x, y)$	y difference pattern amplitude weighting (illumination) function
δ_{xij}	$= \delta_x(x_i, y_j)$
δ_{ij}	Kronecker delta function
ϵ_u, ϵ_v	error in $\sin\alpha$, $\sin\beta$
ϵ_i	differential phase error for bit i

ζ_{mn}	total differential phase error at element mn
λ	wavelength
$\underline{\mu}, \underline{\nu}$	lattice vectors
ξ	element phase error
$\underline{\rho}_{mn}$	position vector of mnth element
ρ	distance from array center
σ_u, σ_v, σ_ξ, σ_ζ	rms error in subscripted variable
ϕ	commanded phase angle
ϕ'	actual phase angle
ϕ_{ci}	commanded phase of ith column for steering in u
ϕ_{rj}	commanded phase of jth row for steering in v
ϕ_{sij}	space feed collimation phase at element ij
ϕ_{oi}	insertion phase of the ith bit in a phase shifter
ϕ_{ij}	commanded phase at element ij

Underlined symbols represent vectors. The non-underlined symbol of a vector quantity represents the scalar magnitude of that vector.

1. INTRODUCTION

The major contributors to angular measurement errors in phased array radars include receiver noise, instrument noise, and target glint. At long range, the errors tend to be dominated by noise at the receiver. At shorter range where the SNR is high, the instrument errors can predominate. At very short range, angular error due to target glint can provide the dominant source of error. Propagation and multipath can also cause substantial errors, but these will not be considered in this paper.

In situations where a radar is used to control the intercept of a target by an interceptor, the SNR at the intercept range is often quite high and object tracking errors tend to be dominated by radar instrument errors. If, furthermore, the same radar is used to track both target and interceptor, fixed or slowly varying instrument bias errors do not, to a first order, affect the error in measuring the relative position of target and interceptor. For such problems it is the randomly varying (i.e., with angle) component of the angular instrument errors which is of greatest concern.

Attention here is thus confined to the randomly varying component of phased array angular instrument errors. The effect of these errors on tracking accuracy depends both on their magnitude and spatial correlation properties, i.e., the manner in which these errors change with beam pointing angle. In many analyses these instrument errors are assumed to be statistically uncorrelated from pulse to pulse. In practice these errors will tend to decorrelate at a rate which depends on the angular rate of the object being tracked. The assumption that these errors are statistically uncorrelated can lead to a serious underestimation of angular tracking errors (and hence interceptor miss distance).

The principal contributors to the random angular instrument errors considered in the analysis are:

a. Finite computation accuracy in the beam steering computer, including word truncation in row and column adders

b. Truncation of steering commands in the digitally controlled array phase shifters

c. Phased array element differential phase errors.

These phase errors in the antenna aperture illumination produce errors in the position of the null in the monopulse difference pattern. An error can also arise from an error in the slope of the monopulse difference pattern, but it will be assumed here that the target being tracked is very close to the null of the difference pattern so that this error can be safely neglected.

The manner in which phase errors influence angular measurement errors depends on the statistical properties of these phase errors across the array face. A spatially periodic behavior in the errors can produce very large angular measurement errors at certain pointing angles. (See, for example, Sec. 7.2 of [1].) It is well known [1], [2] that the use of space feed collimation or the addition of a random phase shift (appropriately compensated in the beam steering command) to each element will tend to smear out these spatial periodicities so that the angular measurement errors do not become very large in certain directions.

Additionally, certain techniques can be employed in the radar to ensure that these errors become largely decorrelated from pulse to pulse. These include the use of angle dithering, frequency dithering and phase dithering. The effectiveness of these dithering techniques has been analyzed with the aid of a specially developed computer program for modeling phased array angular instrument errors. The results are illustrated for a typical phased array configuration.

II. METHOD OF ANALYSIS

Beam steering in a planar phased array antenna is achieved by establishing a linear phase gradient across the aperture which, in turn, provides the desired direction of wave-front propagation. As is expected, amplitude and phase errors across the aperture face will cause errors in both the transmitted wave front direction and the measured angle-of-arrival of reflected energy. Angle-of-arrival of energy reflected from an object is determined by processing both the output of the sum beam and the monopulse difference output [3]. It has been shown by Nester [4] that when amplitude and phase errors across the aperture are small, angle measurement errors are given to a first order by a weighted sum of the phase errors in the monopulse difference pattern illumination function. In particular, Nester's analysis shows that angle measurement errors are independent, to a first order, of sum pattern amplitude and phase errors and difference pattern amplitude errors.

The phase error at each array element in the monopulse difference pattern illumination function consists of a bias component, i.e., insertion phase error, and a variable error which depends on the commanded phase. The insertion phase error, as Nester shows, gives rise to a fixed instrument bias error. Since instrument bias errors are of no concern here, insertion phase errors will be ignored in this paper. The variable phase errors are due to finite computation accuracy in the beam steering computer, truncation of steering commands in the digitally controlled phase shifters, and element differential phase errors. The latter errors are associated with the bit setting of each phase shifter and will be defined, along with the other error sources in Sec. II-C.

A. Phased Array Geometry

The antenna face is assumed to consist of a regular planar lattice of elements. A typical array geometry is shown in Fig. 1. As shown, x and y are orthogonal cartesian coordinates across the aperture face, and the z

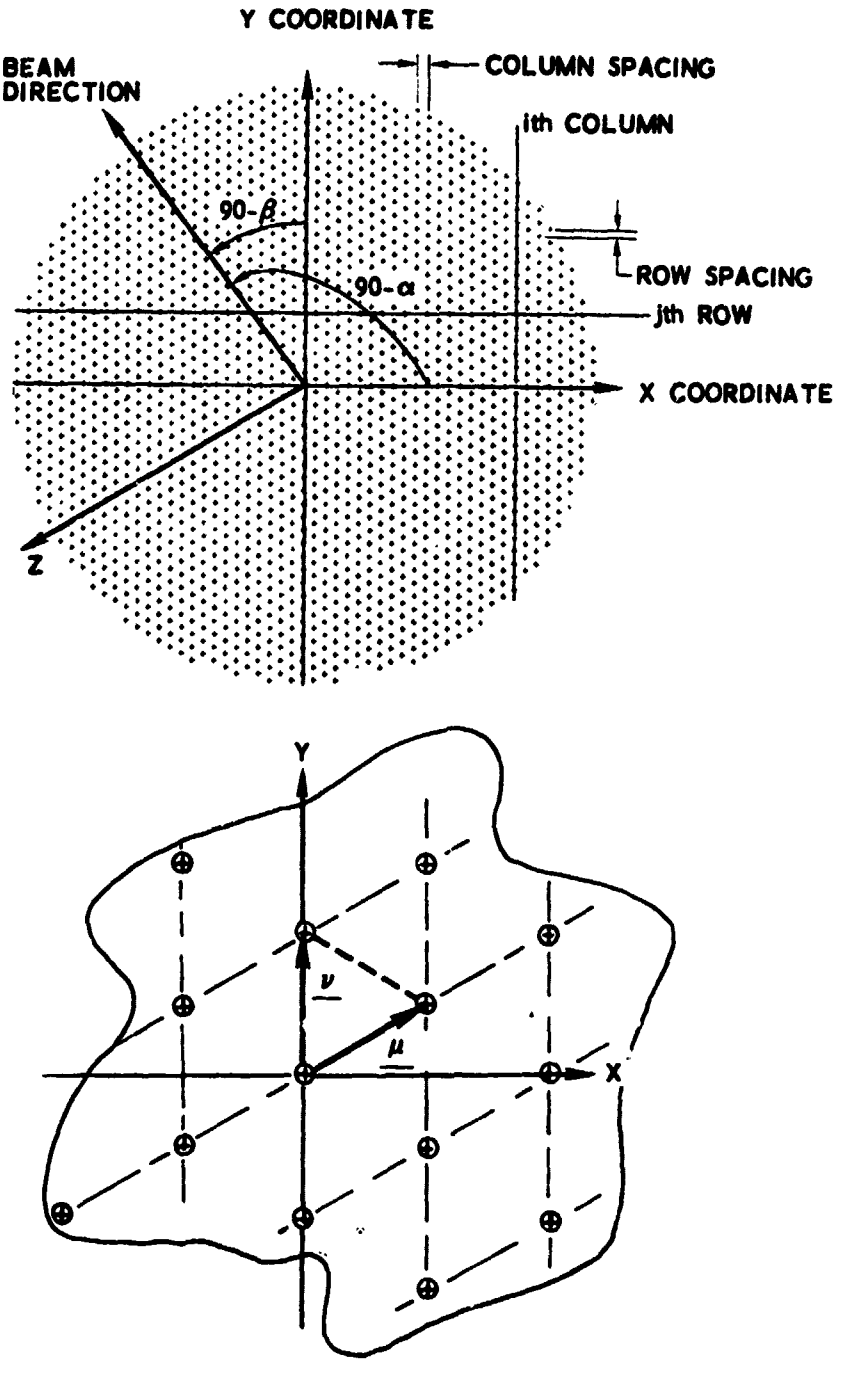

Fig. 1 Phased Array Lattice Geometry

coordinate, normal to the face aperture, is chosen to form a right-handed coordinate system. The element spacing is determined by lattice vectors $\underline{\mu}$ and $\underline{\nu}$ which are not necessarily orthogonal and do not necessarily line up with the x or y axes.

The beam direction is determined by the angles α and β, where α is the angle between the beam and the yz plane, and β is the angle between the beam and the xz plane, as shown in Fig. 1. It is most convenient to express pointing angle by sine coordinates $u = \sin\alpha$ and $v = \sin\beta$. The array in Fig. 1 is shown as circular with an equilateral triangular grid structure, but the method of analysis is not restricted to this case. The geometry of Fig. 1 is assumed for all the cases analyzed in this paper, however.

The position of a given element in the lattice is characterized by indices m and n, and the vector displacement of the mnth element in the aperture face $\underline{\rho}_{mn}$ is given by

$$\underline{\rho}_{mn} = m\underline{\mu} + n\underline{\nu} \quad . \tag{1}$$

The x and y components of the vector $\underline{\rho}_{mn}$ are simply

$$x_{mn} = m\mu_x + n\nu_x \tag{2}$$

$$y_{mn} = m\mu_y + n\nu_y \tag{3}$$

where μ_x and μ_y are the x and y components of $\underline{\mu}$ and ν_x and ν_y are the x and y components of $\underline{\nu}$.

In the lattice structure, the array elements can also be put on a rectangular grid which is lined up with the x and y axes, as shown in Fig. 1. The indices i and j denote the column number and row number of the rectangular grid. When the array lattice is non-rectangular, only certain i j combinations are occupied by phased array elements.

B. Error Formulas

The angular measurement errors are computed from a weighted sum, extending over the aperture, of phase errors at each element, as derived by Nester (see Eq. (60) of Ref. [4]). The two orthogonal angle errors, expressed in sine-space coordinates u and v are[*]

$$\epsilon_u = \frac{\sum_{m,n} \delta_{xmn} \xi_{mn}}{k \sum_{m,n} \delta_{xmn} x_{mn}} \tag{4}$$

$$\epsilon_v = \frac{\sum_{m,n} \delta_{ymn} \xi_{mn}}{k \sum_{m,n} \delta_{ymn} y_{mn}} \quad . \tag{5}$$

The quantities appearing in these expressions are defined as follows:

ϵ_u = error in u

ϵ_v = error in v

$\delta_x(x,y)$ = x monopulse difference pattern amplitude weighting (illumination) function at coordinates x, y

$\delta_y(x,y)$ = y monopulse difference pattern amplitude weighting (illumination) function at coordinates x, y

---

[*] Throughout this analysis pointing angles will be expressed in sine-space coordinates. In particular, the errors ϵ_u and ϵ_v are expressed in millisines (ms).

$\delta_{xmn} = \delta_x(x_{mn}, y_{mn})$

$\delta_{ymn} = \delta_y(x_{mn}, y_{mn})$

$\xi(x, y)$ = phase error at the coordinates x, y

$\xi_{mn} = \xi(x_{mn}, y_{mn})$

k = propagation constant = $\frac{2\pi}{\lambda}$.

Note that δ_x is odd in x but even in y, while δ_y is even in x and odd in y. It is readily apparent from (4) and (5) that a constant phase error across the array face does not contribute to the angular errors. It is evident that once the aperture, i.e., shape, lattice structure, etc., and the difference pattern weighting function have been defined, the only quantities that vary with scan angle are the ξ_{mn}. In particular, the denominators in the above two expressions are merely normalization constants. It is of interest, therefore, to examine the sources of the errors which determine the ξ_{mn}.

C. Scan Dependent Phase Errors

Each digitally controlled phase shifter controls the phase at each element to a binary submultiple of 2π radians, i.e., 180°, 90°, 45°, etc. In practice, each bit of the phase shifter introduces a phase shift, say ϕ_{oi}, in the "off" state and $\phi_{oi} + 2\pi/2^i + \epsilon_i$ in the "on" state where i denotes the bit number, with bit 1 controlling 180°, bit 2 controlling 90° and so on. With all phase shifter bits in the "off" position, the total phase shift is $\Sigma_i \phi_{oi}$. This residual phase is called the insertion phase. This insertion phase, which varies from element to element due to manufacturing tolerances, is independent of phase shifter setting and hence does not change with beam pointing angle. It is readily seen from Eqs. (4) and (5) that these insertion phases introduce fixed bias errors in the angular measurements. Since the constant insertion phase error generates only bias errors, the ϕ_{oi} are taken to be zero. The error ϵ_i represents the phase error corresponding to the ith bit if it is "on." These errors are the differential phase errors and result

from manufacturing tolerances. The statistical properties of these differential phase errors depend, of course, on the manufacturing procedures employed. Since these errors are scan dependent, their contribution to the measurement errors, ϵ_u and ϵ_v, must be taken into account.

A major source of phase error at each array element is due to truncation of the binary phase shift commands in the beam steering computer and at the element phase shifters. In order to determine how these truncation errors affect angle measurement errors, consider how the phase shift commands are generated for each array element. The beam steering command for the ijth element, ϕ_{ij}, is given by the sum

$$\phi_{ij} = \phi_{ci} + \phi_{rj} + \phi_{sij}$$

where

ϕ_{ci} = commanded phase of ith column for steering in u

ϕ_{rj} = commanded phase of jth row for steering in v

ϕ_{sij} = space feed collimation phase at coordinates x_i, y_j.

$\phi_{sij} = 0$ if no space feed collimination is present. The linear phase gradient commands for row and column steering are given in terms of the angle coordinates u and v by

$$\phi_{ci} = kx_iu \tag{6}$$

$$\phi_{rj} = ky_jv \tag{7}$$

where

x_i = horizontal aperture coordinate of the ith column

y_j = vertical aperture coordinate of the jth row.

The space feed collimation phase ϕ_{sij} for the ijth element is determined from

$$\phi_{sij} = k\left[\left(F^2 + x_i^2 + y_j^2\right)^{1/2} - F\right] \tag{8}$$

where F is the focal length of the space feed structure.

In the beam steering computer the quantities ϕ_{ci}, ϕ_{rj}, and ϕ_{sij} are computed to s bits and truncated to r bits. These quantities are then added and the result truncated to q bits, which is the number of bits required to control the phase shifter.

Figure 2 illustrates how these beam steering operations are simulated in the computer error analysis program in order to obtain the element phase shift errors ξ_{mn} which are needed to determine angular errors ϵ_u and ϵ_v. For any chosen lattice points m and n, the row and column indices i and j are computed with the aid of (2) and (3). ϕ_{ci} and ϕ_{rj} are then computed from (6) and (7) using the commanded pointing angles u and v and the cartesian coordinates of the elements x_i and y_j. If present, the collimation phase is readily calculated from (8). The row and column addition indicated is performed as described above and the result is truncated to q bits. The box labeled "compute differential phase error, etc." represents a bit-testing function that senses the phase shifter bit setting and determines which bits are "on." In the computer simulation, the differential phase error for each bit in the array is separately generated with the aid of a random number generator and stored for use by the program. For each bit that is "on," the corresponding differential phase error is recalled from storage and added to the phase developed at the phase shifters. Comparing the phase thus actually developed with the desired phase, results in the elemental phase error, ξ_{mn}.

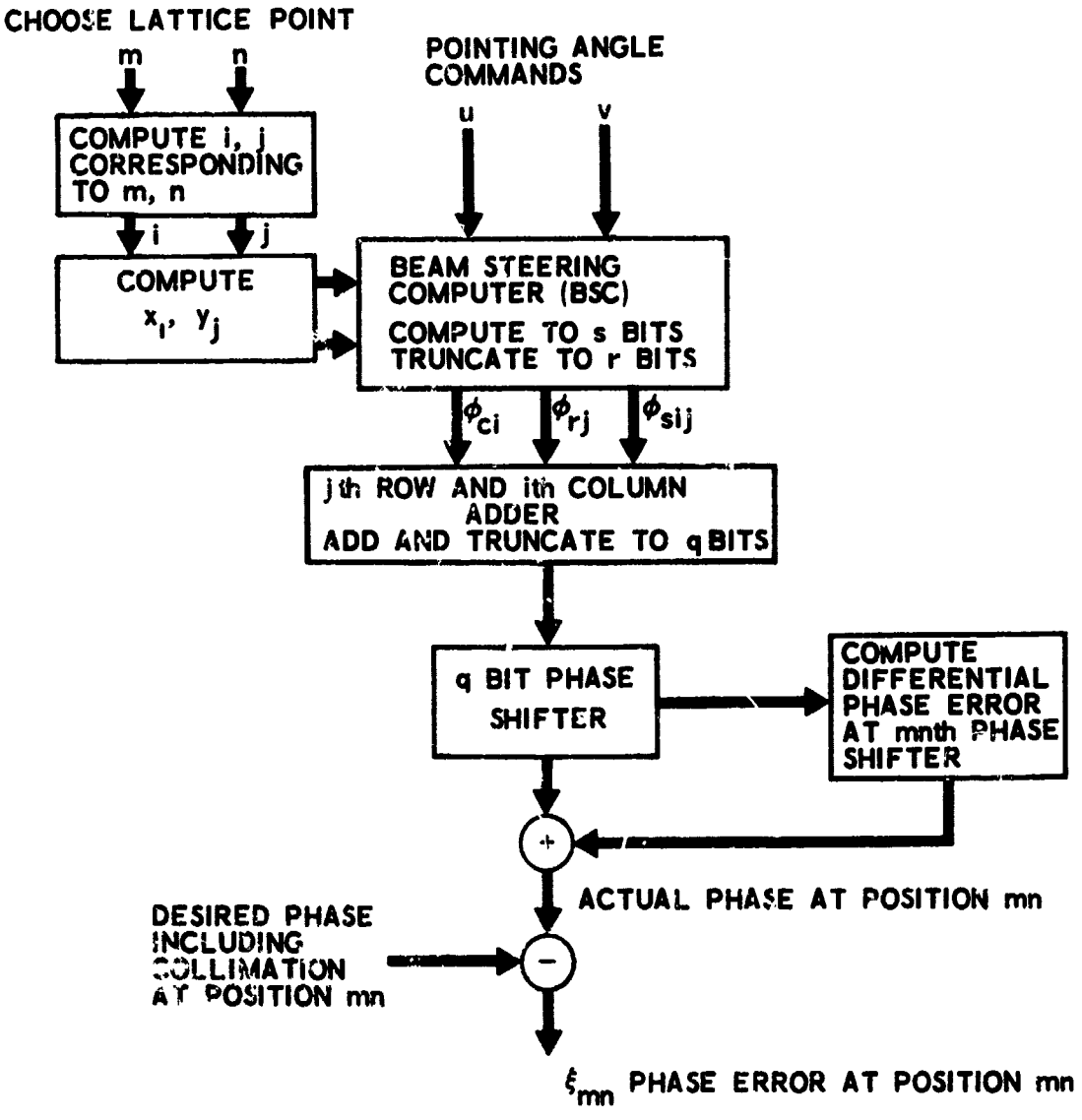

Fig. 2 Simulation of Beam Steering Computer Logic

Reference to Fig. 2 shows that the collimation angle ϕ_{sij} has to be computed or recalled many times, typically once for each phase shifter element. It has been shown by Hatcher [5] that this computation can be simplified considerably by expanding this collimation term as a sum of two terms where the first depends only on x_i and the second only on y_j. This procedure reduces the number of collimation computations to the sum of the number of rows and columns. The expression for the collimation phase can be expanded in a Taylor series:

$$\phi_{sij} = \frac{\pi}{\lambda F}\left(x_i^2 + y_j^2\right) + \text{higher order terms of even powers of } x_i \text{ and } y_j$$

Thus $\phi_{sij} \simeq \phi_{si} + \phi_{sj}$, where $\phi_{si} = \pi x_i^2/\lambda F$ and $\phi_{sj} = \pi y_j^2/\lambda F$. The summation of the higher order terms, which are even powers of x_i and y_j, weighted by the odd difference pattern illumination functions, vanishes identically in the calculation of ϵ_u and ϵ_v as defined by Eqs. (4) and (5). Thus the omission of these higher order terms does not contribute to the angular errors but does produce some degradation in main beam gain and sidelobe levels, as discussed by Hatcher [5]. Nevertheless, this degradation does not prove to be serious in most situations of interest. A schematic diagram of this mode of operation is shown in Fig. 3. The quantities ϕ_{ci}, ϕ_{rj}, ϕ_{si}, and ϕ_{sj} are computed in the beam steering computer to an accuracy of s bits. The row and column commands are then added and truncated to r bits. From this point on, the sequence of operations in Fig. 3 is identical to that of Fig. 2.

The approximate method for calculating the collimation phase as described above was used for all applicable cases analyzed in this paper.

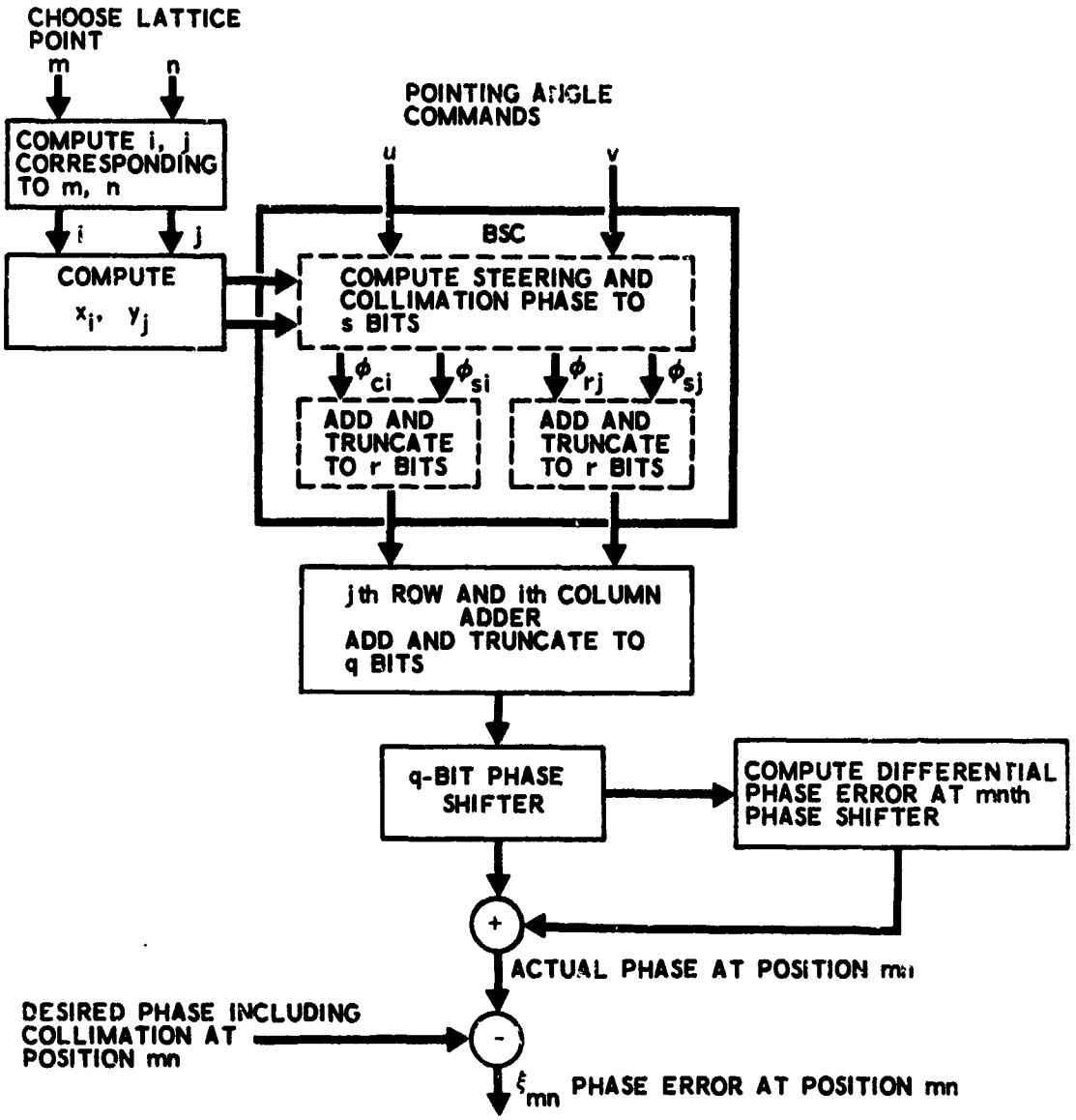

Fig. 3 Simulation of Beam Steering Computer Logic with Simplified Collimation Commands

D. Randomized Quantization Levels

A q bit phase shifter has uniformly spaced quantization levels (ignoring differential phase errors) with spacing

$$Q = \frac{\pi}{2^{q-1}} \quad .$$

The generation of phase shifter quantization errors is illustrated in Fig. 4. The solid line represents the desired phase. The dashed staircase function is the actual phase due to quantization. The difference between these functions gives a periodic sawtooth error with amplitude Q/2. This sawtooth is an odd function of commanded phase. An error of this type results wherever a binary number representing phase is truncated.

In the situation where a linear phase function is applied across the aperture face, quantization errors will cause errors which will be periodic across the face of the aperture. As noted earlier, spatially periodic phase errors produce angle measurement errors in certain directions which can be quite large. It is well known that the space feed collimation correction tends to smear out these periodicities and thereby substantially reduces the maximum angular error [1], [2]. A more direct approach sometimes employed on corporate fed arrays is to deliberately vary the starting position (but not the spacing) of the quantization levels in a random way from element to element. This randomization may be implemented in some types of arrays by randomizing the length of cable (or waveguide) which drives each element of the array, and compensating for the differential delay path by adding an appropriate compensation phase number to the commanded phase for each element at a point prior to truncation of the beam steering command in the q bit phase shifters.

The dramatic improvement in accuracy which results with the use of randomized quantization levels is illustrated schematically for a worst case situation in Fig. 5. To simplify the illustration, a one-dimensional case has been considered where the desired phase is a linear function of the

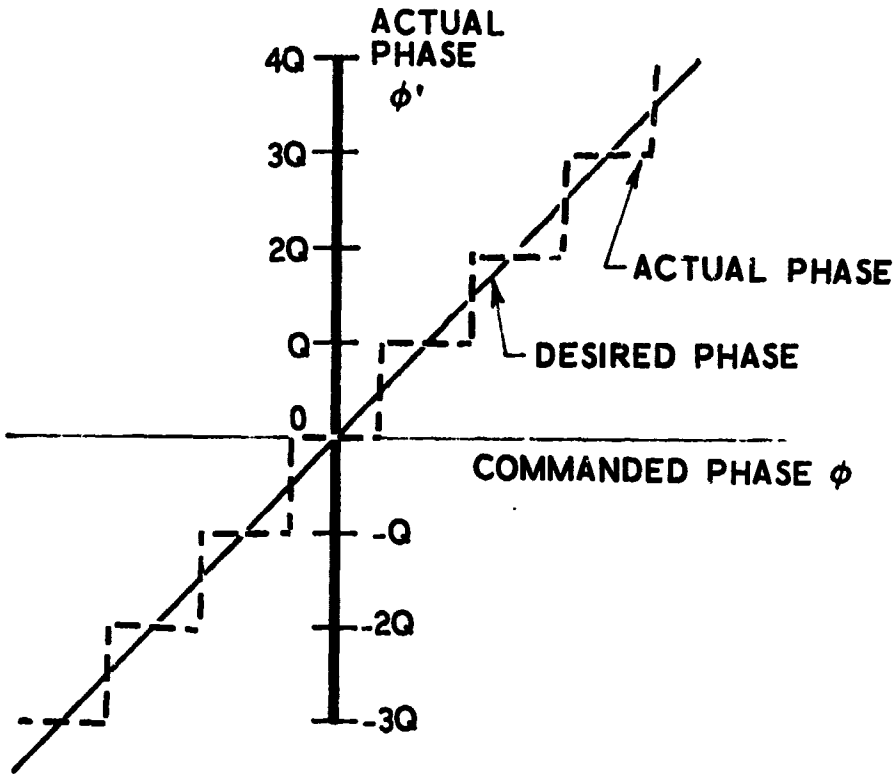

Fig. 4 Phase Shifter Quantization Errors

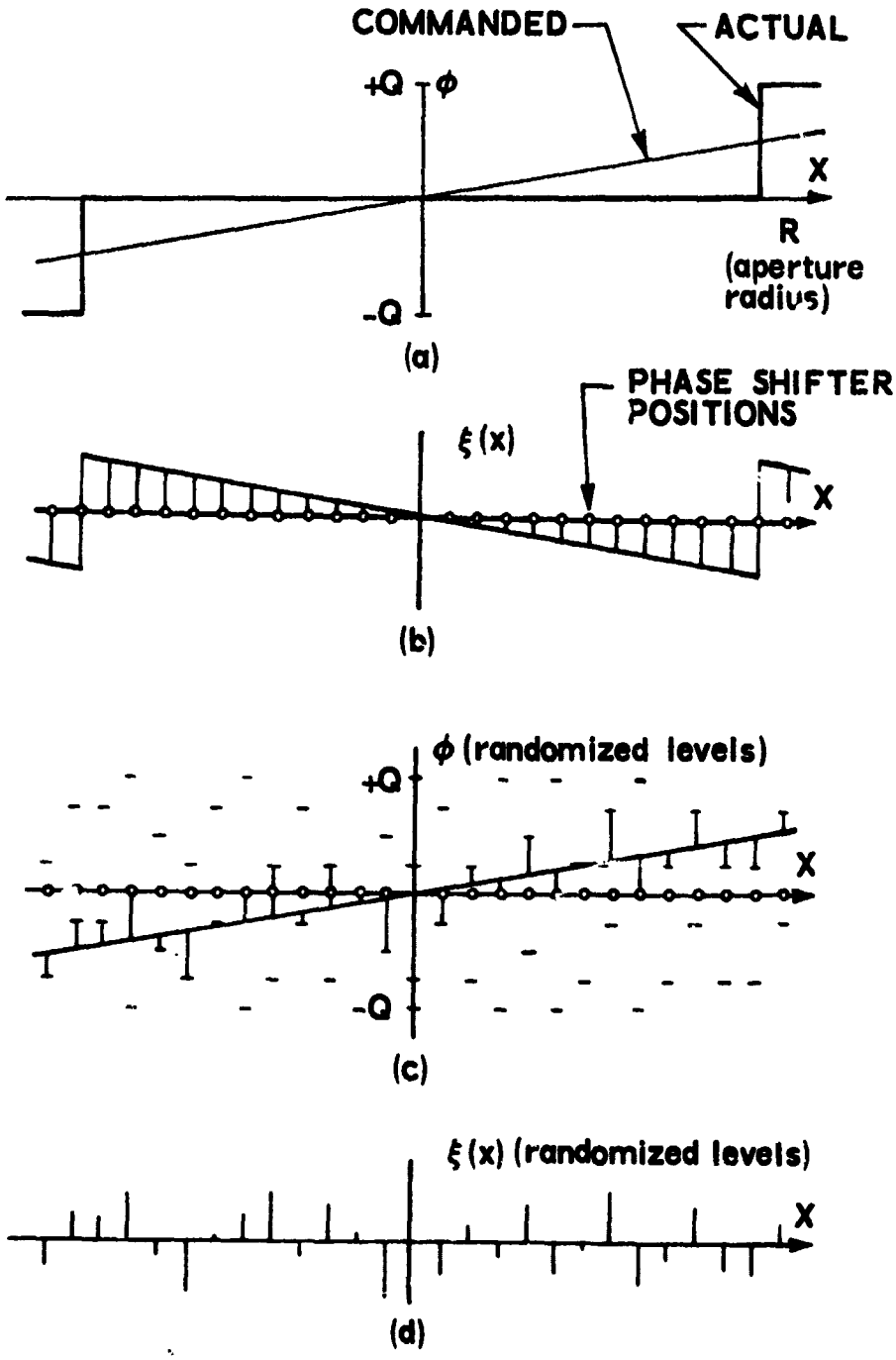

Fig. 5 Randomization of Worse Case Quantizing Errors

aperture coordinate x. As illustrated in (a), the beam steering off the array normal is small, and the commanded phase causes only the phase shifters at the very edge of the aperture to switch out of the zero state. As seen from part (b), the difference between the commanded and actual phase functions is a linear phase error term which will cause an angular error approximately equal to the commanded steering angle. Part (c) of the figure illustrates the effect of randomized quantization levels. The horizontal dashes indicate the location of the nearest quantization levels for each phase shifter. In all cases, the commanded phase is quantized to the nearest available quantization level. The resulting phase errors at each phase shifter, shown in part (d) of the figure, are seen to have a random character which will not give rise to a large angular error.

E. Evaluation of the RMS Angular Error

A formula for the rms angular error is developed in this section for the case where phase shifter phase errors are spatially uncorrelated. The assumption of uncorrelated errors is valid only if some means of phase randomization exists, such as the method of randomized quantization levels discussed in the previous section. Space feed collimation also provides a form of spatial decorrelation, although regions of correlation remain, as will be discussed later. The condition for uncorrelated phase errors is given by

$$\overline{\xi_{mn}\xi_{m'n'}} = \sigma_{\xi}^{2}\delta_{mm'}\delta_{nn'}$$

where the bar denotes mathematical expectation (in this case an ensemble average) and δ_{ij} is the Kronecker delta function. For the error sources considered, the mean square phase error σ_{ξ}^{2} is the same for all elements.

From Eq. (4), noting that $\bar{\xi}_{mn} = 0$ (since insertion phase errors have been set to zero), it follows that $\bar{\epsilon}_u = 0$. The variance of u, σ_u^2 is then given by

$$\sigma_u^2 = \overline{\epsilon_u^2} = \frac{\sigma_\xi^2 \sum_{m,n} \delta_{xmn}^2}{k^2 \left(\sum_{m,n} \delta_{xmn} x_{mn} \right)^2} \quad . \tag{9}$$

An exactly analogous expression can be derived for σ_v^2

$$\sigma_v^2 = \overline{\epsilon_v^2} = \frac{\sigma_\xi^2 \sum_{m,n} \delta_{ymn}^2}{k^2 \left(\sum_{m,n} \delta_{ymn} y_{mn} \right)^2} \quad . \tag{10}$$

These expressions are easily evaluated numerically. Values of σ_u^2 and σ_v^2 computed for various difference pattern weighting functions are given in Appendix A. The estimates of variance from computer simulation generated sequences of ϵ_u and ϵ_v are in excellent agreement with values calculated from the above formulas in those cases where quantization level randomization or space feed collimation is employed.

III. PERIODICITY AND SYMMETRY PROPERTIES OF ANGULAR ERRORS

In this section we shall derive some of the more useful periodicity and symmetry properties obeyed by the phased array angle measurement errors. These properties aid in the interpretation of computed error functions and enable the amount of computation to be substantially reduced. These properties arise from periodic behavior of the array lattice, the particular symmetry properties of the lattice structure considered, and the symmetry and periodicity properties of phase errors due to truncation of binary steering commands in each element phase shifter.

In addition to the lattice properties specified by the lattice vectors $\underline{\mu}$ and $\underline{\nu}$, we make use of the following relationships:

$$\delta_x(x, y) = \delta_x(x, -y) = -\delta_x(-x, y) \tag{11}$$

$$\delta_y(x, y) = \delta_y(-x, y) = -\delta_y(x, -y) \tag{12}$$

and, as seen from Fig. 4,

$$\xi(\phi) = -\xi(-\phi) \tag{13}$$

$$\xi(\phi) = \xi(\phi + Q) \tag{14}$$

where ξ is the phase shifter quantization error (in the absence of quantization level randomization) and ϕ is the commanded phase. The commanded phase at the point (x, y) for a commanded angle (u, v) is, ignoring collination,

$$\phi = k(xu + yv) \quad . \tag{15}$$

With these relationships, Eqs. (4) and (5) can be put in the following form, where proportionality constants have been omitted:

$$\epsilon_u(u, v) \sim \sum_{m, n} \delta_x(x_{mn}, y_{mn})\ \xi\left[k(x_{mn}u + y_{mn}v)\right] \tag{16}$$

$$\epsilon_v(u, v) \sim \sum_{m, n} \delta_y(x_{mn}, v_{mn})\ \xi\left[k(x_{mn}u + y_{mn}v)\right] \quad . \tag{17}$$

These relationships are now in a convenient form for deriving the desired properties of the error functions.

Let $\underline{w}$ be a vector with components (u, v). $\underline{w}$ represents a vector pointing angle in (u, v) space. Periodicities in (u, v) space are found by determining values of $\Delta\underline{w}$ which leave ϵ_u and ϵ_v unchanged. It can be verified by direct substitution in the above equations that displacements $\Delta\underline{w} = \underline{U}$ and $\Delta\underline{w} = \underline{V}$ leave ϵ_u and ϵ_v unchanged, where

$$\underline{U} = \frac{Q(\underline{\nu} \times (\underline{\mu} \times \underline{\nu}))}{k(\underline{\nu} \times \underline{\mu})\cdot(\underline{\nu} \times \underline{\mu})} = \frac{Q(\nu^2\underline{\mu} - (\underline{\mu}\cdot\underline{\nu})\underline{\nu})}{k(\mu^2\nu^2 - (\underline{\mu}\cdot\underline{\nu})^2)} \tag{18}$$

$$\underline{V} = \frac{Q(\underline{\mu} \times (\underline{\nu} \times \underline{\mu}))}{k(\underline{\nu} \times \underline{\mu})\cdot(\underline{\nu} \times \underline{\mu})} = \frac{Q(\mu^2\underline{\nu} - (\underline{\mu}\cdot\underline{\nu})\underline{\mu})}{k(\mu^2\nu^2 - (\underline{\mu}\cdot\underline{\nu})^2)} \quad . \tag{19}$$

Writing $\epsilon_u(u, v) = \epsilon_u(\underline{w})$, it follows that

$$\epsilon_u(\underline{w} + m'\underline{U} + n'\underline{V}) = \epsilon_u(\underline{w}) \tag{20}$$

for arbitrary integers m' and n', and any $\underline{w}$. Similarly

$$\epsilon_v(\underline{w} + m'\underline{U} + n'\underline{V}) = \epsilon_v(\underline{w}) \quad . \tag{21}$$

Thus, the lattice periodicity of the array leads to a lattice periodicity in the error functions ϵ_u and ϵ_v characterized by the lattice vectors $\underline{U}$ and $\underline{V}$. It can be readily shown, in particular, that an equilateral triangle lattice gives rise to angle error functions which also have an equilateral triangle lattice structure.

Consider now the symmetry properties of ϵ_u and ϵ_v in (u, v) space. Using (13) together with (16) readily gives

$$\epsilon_u(-u, -v) = -\epsilon_u(u, v) \quad . \tag{22}$$

Similarly,

$$\epsilon_v(-u, -v) = -\epsilon_v(u, v) \quad . \tag{23}$$

These relations can be written more concisely as

$$\epsilon_u(-\underline{w}) = -\epsilon_u(\underline{w}) \tag{24}$$

$$\epsilon_v(-\underline{w}) = -\epsilon_v(\underline{w}) \quad . \tag{25}$$

Equations (24) and (20) can be combined to give

$$\epsilon_u\left(\frac{m'}{2}\underline{U} + \frac{n'}{2}\underline{V} + \underline{w}\right) = -\epsilon_u\left(\frac{m'}{2}\underline{U} + \frac{n'}{2}\underline{V} - \underline{w}\right) \tag{26}$$

and

$$\epsilon_v\left(\frac{m'}{2}\,\underline{U} + \frac{n'}{2}\,\underline{V} + \underline{w}\right) = -\epsilon_v\left(\frac{m'}{2}\,\underline{U} + \frac{n'}{2}\,\underline{V} - \underline{w}\right) \tag{27}$$

for arbitrary integers m' and n'. The error functions thus have anti-symmetry points about the basic lattice points and mid-lattice points (i.e., midway between lattice points) of the error surface.

Consider, finally, array lattices which have reflection symmetry about the x and y axes. The triangular lattice shown in Fig. 1 is an example of such a lattice. Then if we replace x_{mn} by $-x_{mn}$ and/or y_{mn} by $-y_{mn}$ everywhere in the array, the lattice structure remains unchanged. Replacing x_{mn} by $-x_{mn}$ in (16) yields, using (11),

$$\epsilon_u(u, v) = -\epsilon_u(-u, v) \quad . \tag{28}$$

Replacing y_{mn} by $-y_{mn}$ in (16) yields, using (11),

$$\epsilon_u(u, v) = \epsilon_u(u, -v) \quad . \tag{29}$$

In a similar manner one can show

$$\epsilon_v(u, v) = \epsilon_v(-u, v) \tag{30}$$

and

$$\epsilon_v(u, v) = -\epsilon_v(u, -v) \quad . \tag{31}$$

For the particular lattice structure shown in Fig. 1, the vector $\underline{U}$ is aligned with the u axis. For an arbitrary integer m' it follows that

$$\epsilon_u(u + m'U, v) = \epsilon_u(u, v) \quad . \tag{32}$$

Combining this with (28) gives

$$\epsilon_u\left(\frac{m'}{2} U + u, v\right) = -\epsilon_u\left(\frac{m'}{2} U - u, v\right) \quad . \tag{33}$$

One can show in a similar manner

$$\epsilon_v\left(\frac{m'}{2} U + u, v\right) = \epsilon_v\left(\frac{m'}{2} U - u, v\right) \quad . \tag{34}$$

Additional symmetry relationships could certainly be derived using similar methods.

It can be shown that properties of the error functions derived above still remain valid if a space feed collimation term is included. These properties will be destroyed, however, by the inclusion of quantization level randomization or element differential phase errors or both.

IV. ARRAY ASSUMPTIONS AND FORMAT OF COMPUTATIONAL RESULTS

The array example used in this paper is a circular array with an equilateral triangle lattice structure, as shown in Fig. 1. The array parameters, as given below, are representative of those which have been considered for command guidance intercept applications.

d_x	(column spacing)	= 0.500 λ
d_y	(row spacing)	= 0.289 λ
μ_x	(lattice parameter)	= 0.500 λ
μ_y	(lattice parameter)	= 0.289 λ
ν_x	(lattice parameter)	= 0.000λ
ν_y	(lattice parameter)	= 0.578 λ
D	(aperture diameter)	= 26.4 λ
R	(aperture radius)	= D/2 = 13.2 λ
N	(number of elements)	= 1891
δ_x	(difference pattern amplitude weighting function)	= sin πx/R
δ_y	(difference pattern amplitude weighting function)	= sin πy/R
F	(focal length in the space feed mode)	= D
q	(no. of phase shifter bits)	= 3

The boresight beamwidth of this array is approximately 2.6°.

The computer error analysis program produces graphs of the angle error ϵ_u and ϵ_v as a function of u and v, and an autocorrelation function of these errors, denoted $R_u(\Delta u, \Delta v)$ and $R_v(\Delta u, \Delta v)$, plotted as a function of differential steering angle, Δu and Δv. The sample point spacing for the simple planar cuts was chosen to be 0.25 ms. The computed rms value of the angular error annotated on each graph refers only to the scan sector actually shown. Unless otherwise indicated, the differential phase errors are set equal to zero for reasons to be discussed later.

Many of the plots shown in the subsequent section are perspective views of the angle errors and the corresponding two-dimensional autocorrelation function. In each of these cases, the sample point spacing was chosen to be 0.5 ms in both u and v. The properties of this perspective plot are illustrated in Fig. 6. Each of the perspective plots is viewed at 60° clockwise from the u axis at an elevation angle of 35°. The limits indicated in the figure are

$$\left\{ \begin{matrix} u_o \\ \Delta u_o \end{matrix} \right\} = \left\{ \begin{matrix} v_o \\ \Delta v_o \end{matrix} \right\} = \left\{ \begin{matrix} \text{20 ms for error surfaces} \\ \text{15 ms for autocorrelation surfaces} \end{matrix} \right.$$

The computation scan is performed parallel to the u axis at constant v, similar to an ordinary raster scan. The 6400 point error surface thus obtained was used to compute the corresponding autocorrelation functions. The plotting lines are drawn at the computation interval, viz., 0.5 ms. Edge effects were neglected in the computation of these autocorrelation functions, which were generated by incrementing Δu and Δv in one quadrant only. Points in the remaining quadrants were obtained by symmetrically transposing points about the origin as justified by symmetry properties of the autocorrelation function.

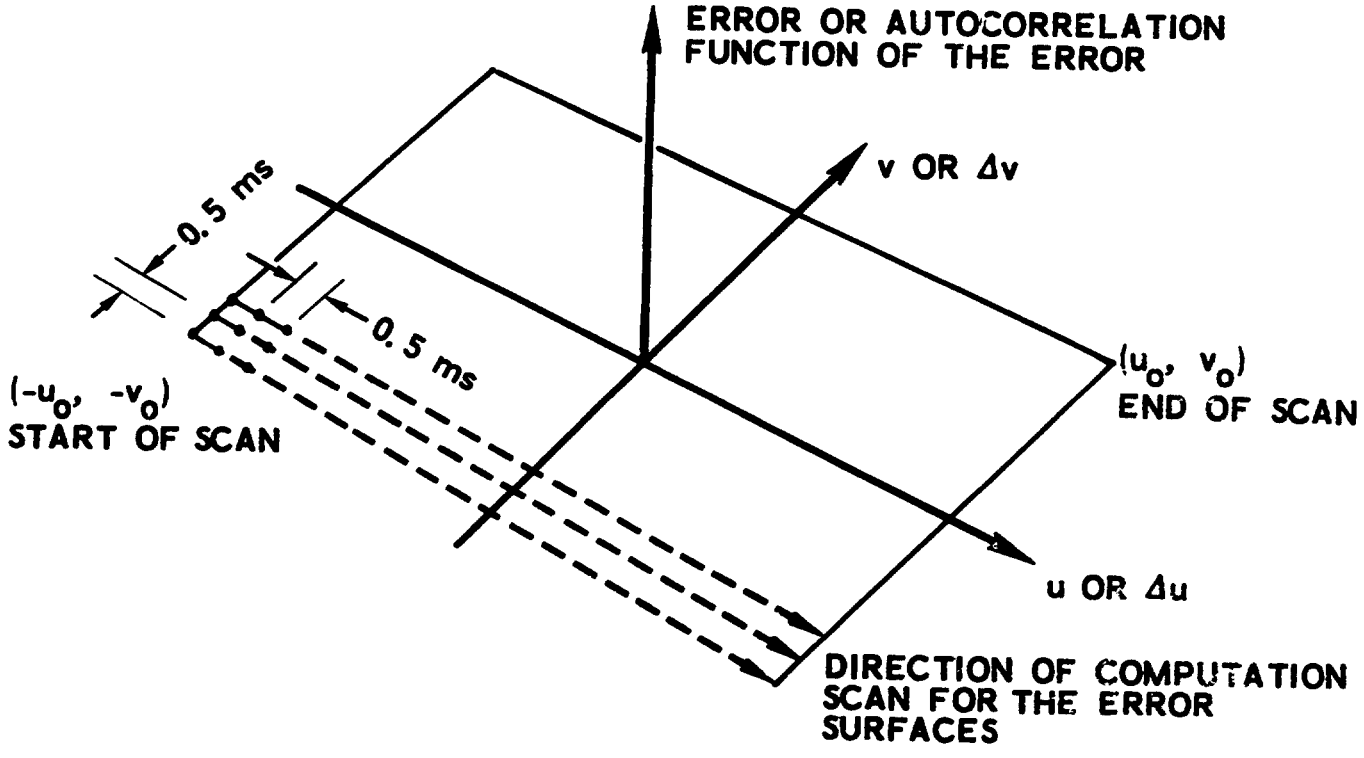

Fig. 6 Perspective Views

The computer error analysis program is written in FORTRAN for use on the IBM 370/155. Special truncation and bit sensing functions that operate on the binary representation of words are required. Because of the 32-bit word structure peculiar to this machine, reference phases are computed to 24 bits, i.e., the quantization step size of computed phase errors is $2\pi/2^{24}$. The amount of storage required for any particular array lattice is given approximately by 3N 32-bit words plus N(2 + q) 16-bit words. Execution time is approximately 120N μsec to compute both ϵ_u and ϵ_v for one beam position and 3-bit phase shifters, including differential phase errors.

A. Quantization Lobes

In the absence of quantization level randomization and space feed collimation, the angle error exhibits large peak values, called quantization lobes, near the array normal and at integral multiples of the error periods U, V. These lobes in the sine alpha error ϵ_u, which are not unlike grating lobes, are apparent in the computer generated plot, Fig. 7. Note the linear portion of ϵ_v with slope of -1 in the region $-5 < u < +5$ ms. In this region, all phase shifter phase commands are smaller than half the quantization level spacing Q. Since none of the phase shifters switches out of the zero state, the resulting error is the negative of the commanded steering angle. The angle at which the magnitude of the error reaches a peak is approximately where the phase shifters at the edge of the array just start to switch into the first quantizing level. The values of u for which this maximum occurs is given approximately by $|u| \approx \max |\epsilon_u| \approx 5$ ms. The normalized autocorrelation function of ϵ_u is shown on the right side of Fig. 7. The autocorrelation function and the rms error in Fig. 7 are not representative of the large sector average due to the predominance of the large peak in the sample interval. Figures 8 and 9 show the two-dimensional error surfaces $\epsilon_u(u, v)$ and $\epsilon_v(u, v)$, respectively. Note that the curve in Fig. 7 represents a planar cut through the surface $\epsilon_u(u, v)$ of Fig. 8 normal to the v axis and at $v = 0$. The symmetry properties as discussed in Sec. III are clearly visible in both ϵ_u and ϵ_v.

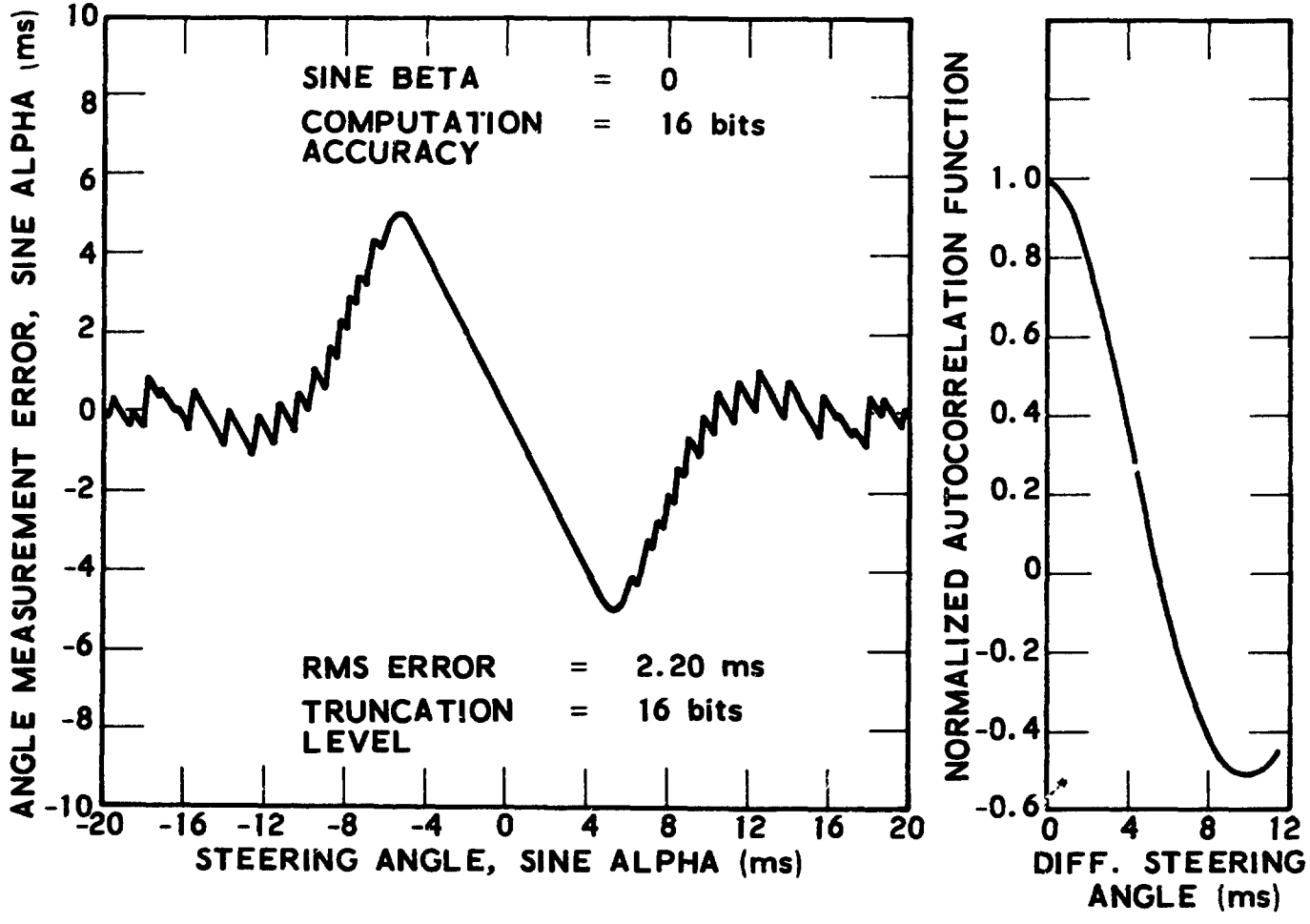

Fig. 7 Sine Alpha Error Illustrating Phase Shifter Quantization Lobes in a Principal Plane Cut

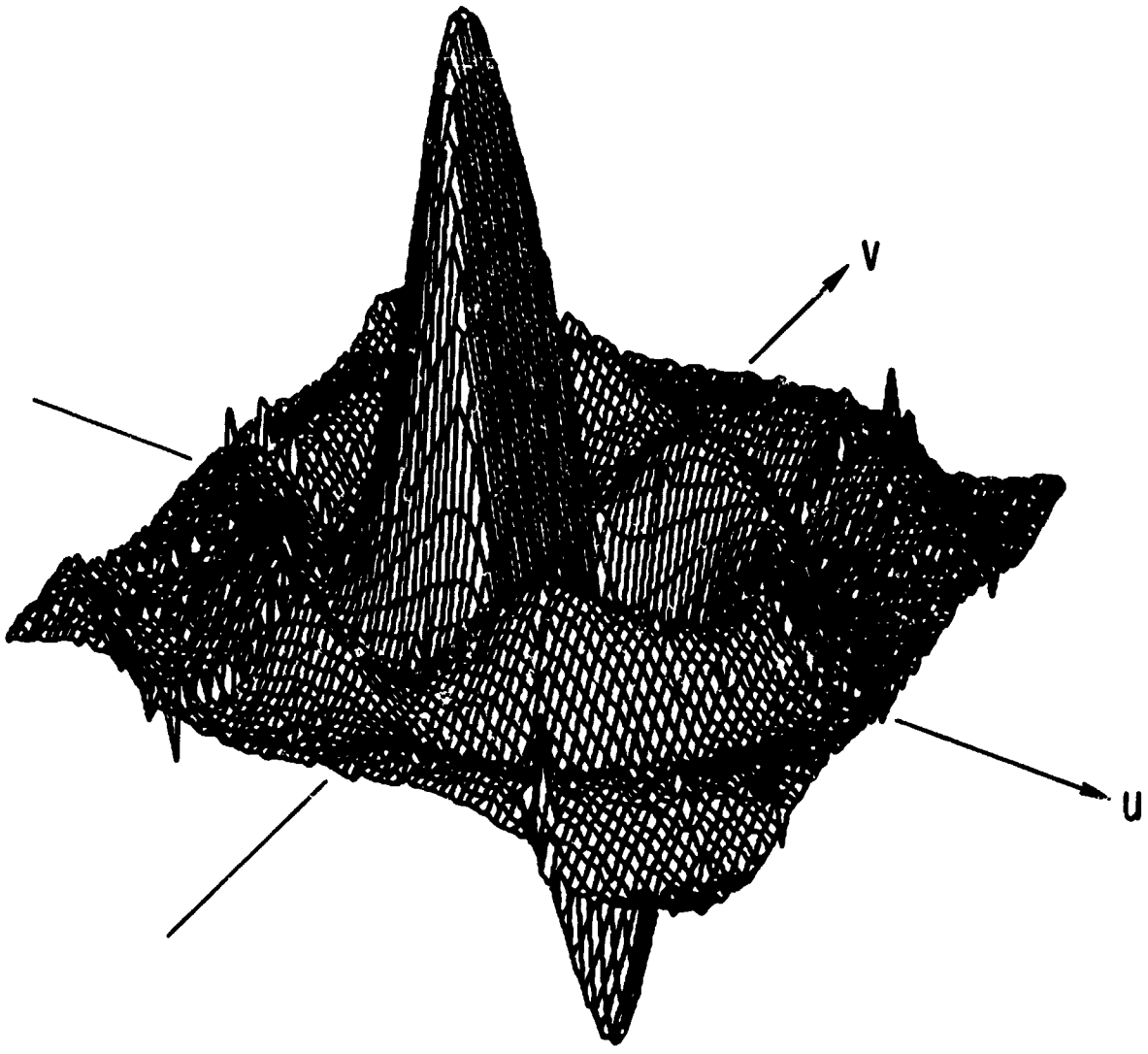

Fig. 8 Perspective View of the Sine Alpha Error Illustrating Phase Shifter Quantization Lobes

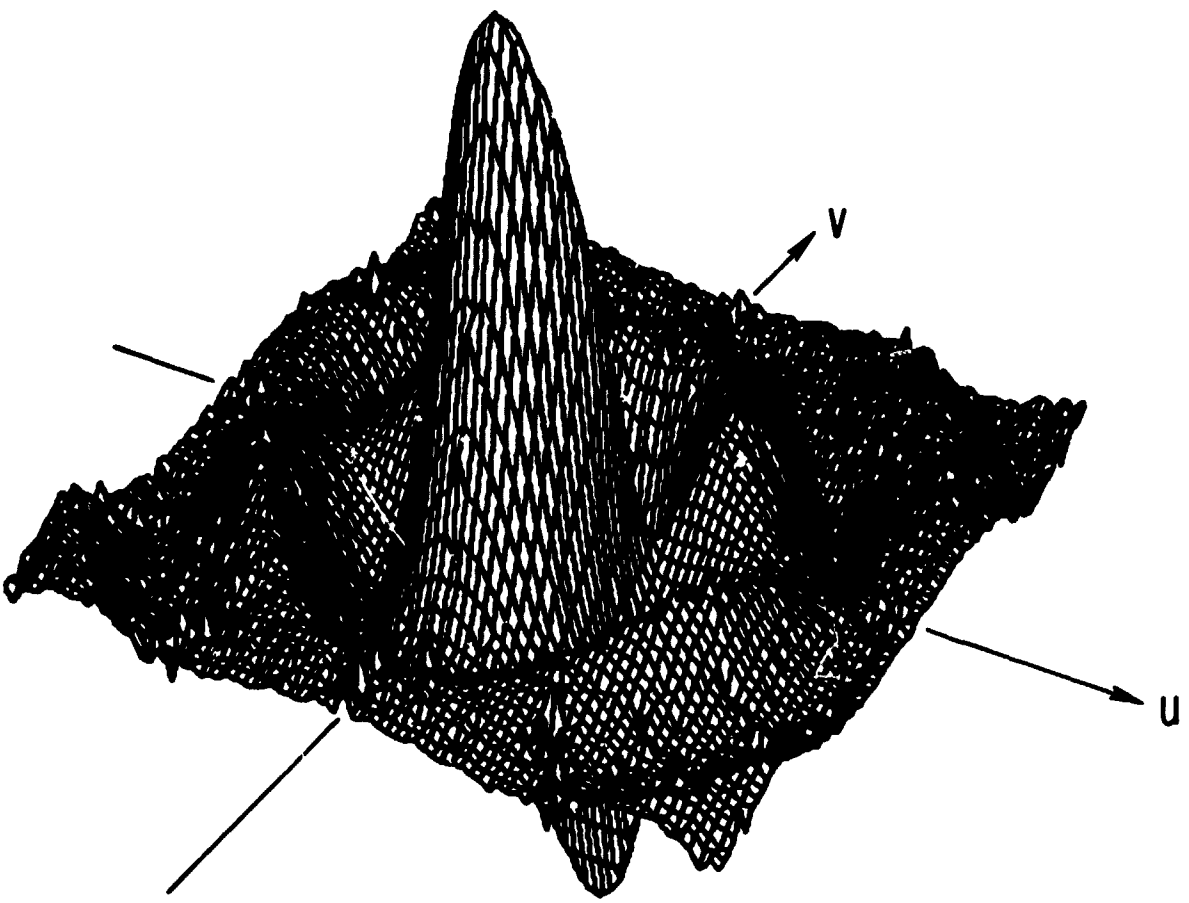

Fig. 9 Persepctive View of the Sine Beta Error Illustrating Phase Shifter Quantization Lobes

B. Addition of Space Feed Collimation

The case presented in Fig. 10 is exactly the same as the case presented in Fig. 7 except that space feed compensation has been included. The collimation was computed on a row and column basis as discussed in Sec. II-C. In comparing this figure to Fig. 7, it is noted that, in addition to a 10:1 change in vertical scale, the resulting error is much more "random." As expected, the error function is still anti-symmetric about the origin, as discussed in Sec. III. The autocorrelation function exhibits a 3 dB width of about 1.7 ms. The rms error is found to be 0.149 ms, which happens to agree well with the predicted large sector rms value of 0.1486 ms calculated from Eq. (9). In the case of the sine beta error, ϵ_v, which is symmetric about the origin, the rms error is 0.203 ms, which compares with a value of 0.148 ms calculated from Eq. (10). This apparent discrepancy is due to the fact that the space feed collimation is not completely effective in randomizing phase errors across the array face. Phase errors of neighboring elements still tend to be correlated. Thus the rms angular errors calculated from a limited scan sector cannot be expected to conform closely with errors predicted from Eqs. (9) and (10).

Figure 11 is the sine alpha error surface in the vicinity of the array normal and shows the same scanning region as Fig. 8 and 9. This figure shows that $\epsilon_u(u, v)$ is zero whenever u is zero, consistent with the anti-symmetry properties discussed in Sec. III. In fact, careful inspection of Fig. 11 reveals the presence of other symmetry properties as discussed in Sec. III. Figure 12 is the two-dimensional autocorrelation function $R_u(\Delta u, \Delta v)$ of $\epsilon_u(u, v)$, i.e., of the error surface shown in Fig. 11. The shape of $R_v(\Delta u, \Delta v)$ is generally similar. This autocorrelation function, as well as the one shown in Fig. 10, shows significant spatial correlation for differential angles of 2 ms and beyond. This spatial correlation could significantly degrade radar performance for applications such as command guidance intercept.

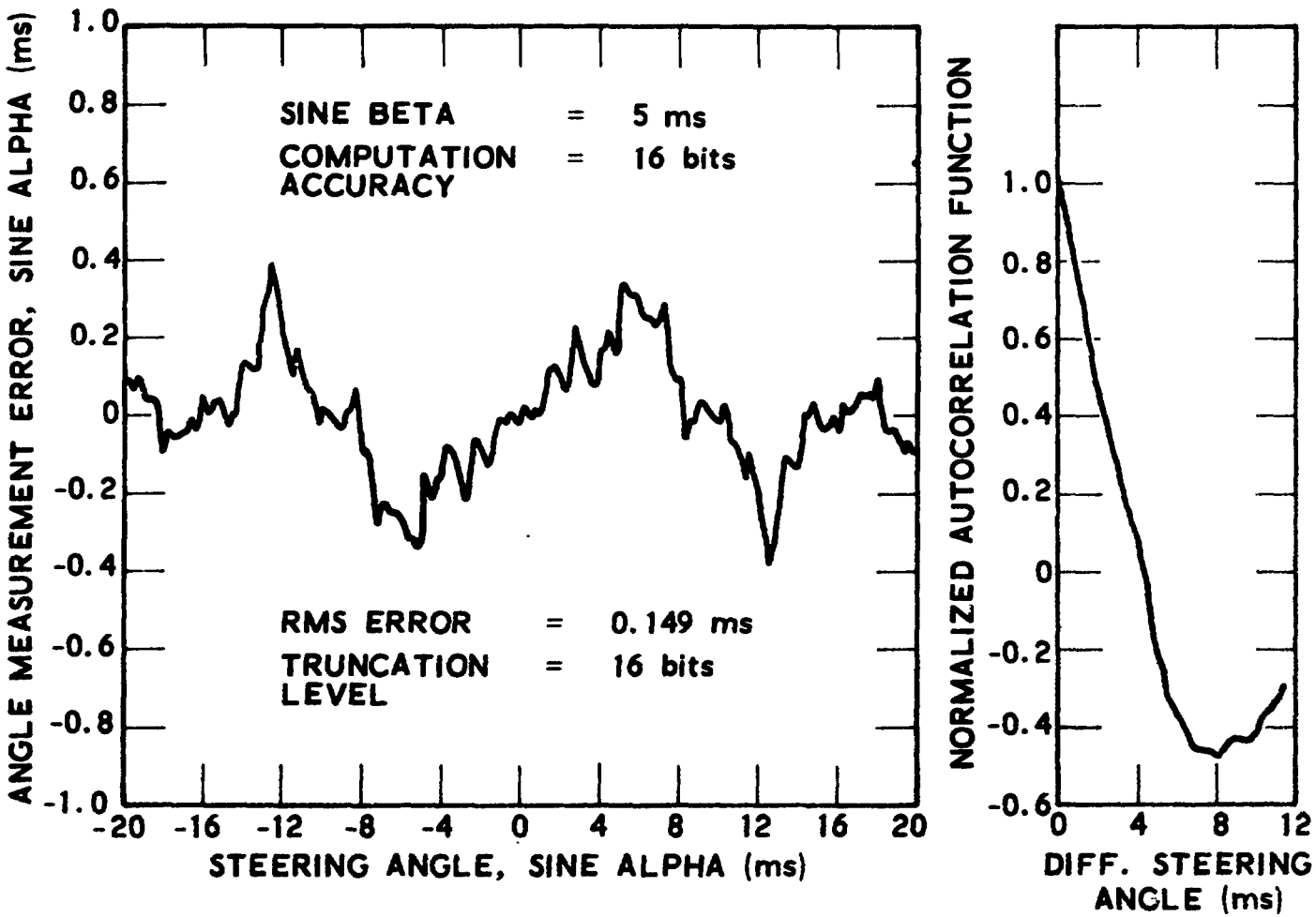

Fig. 10 Sine Alpha Error in the Presence of Row and Column Collimation

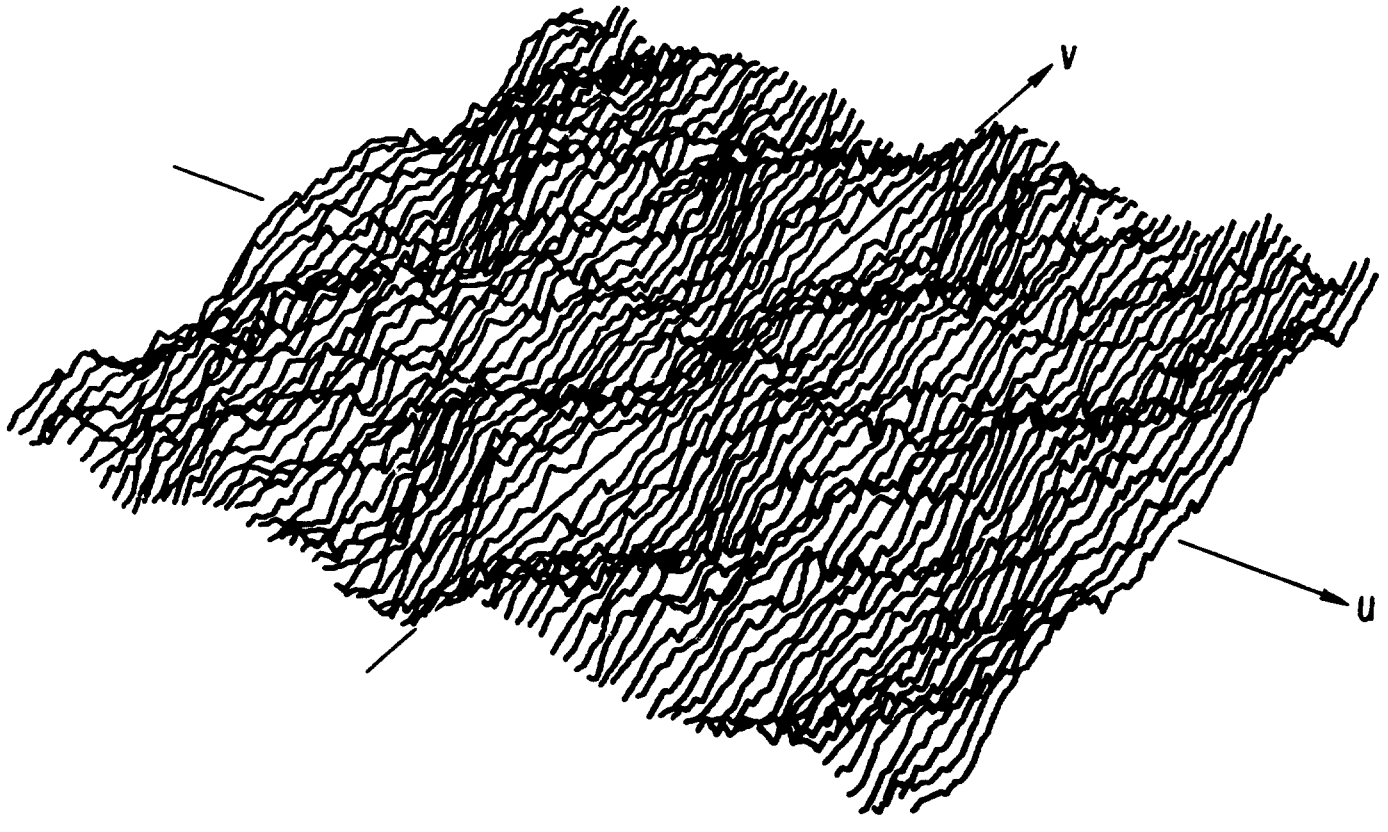

Fig. 11 Perspective View of the Sine Alpha Error in the Presence of Collimation

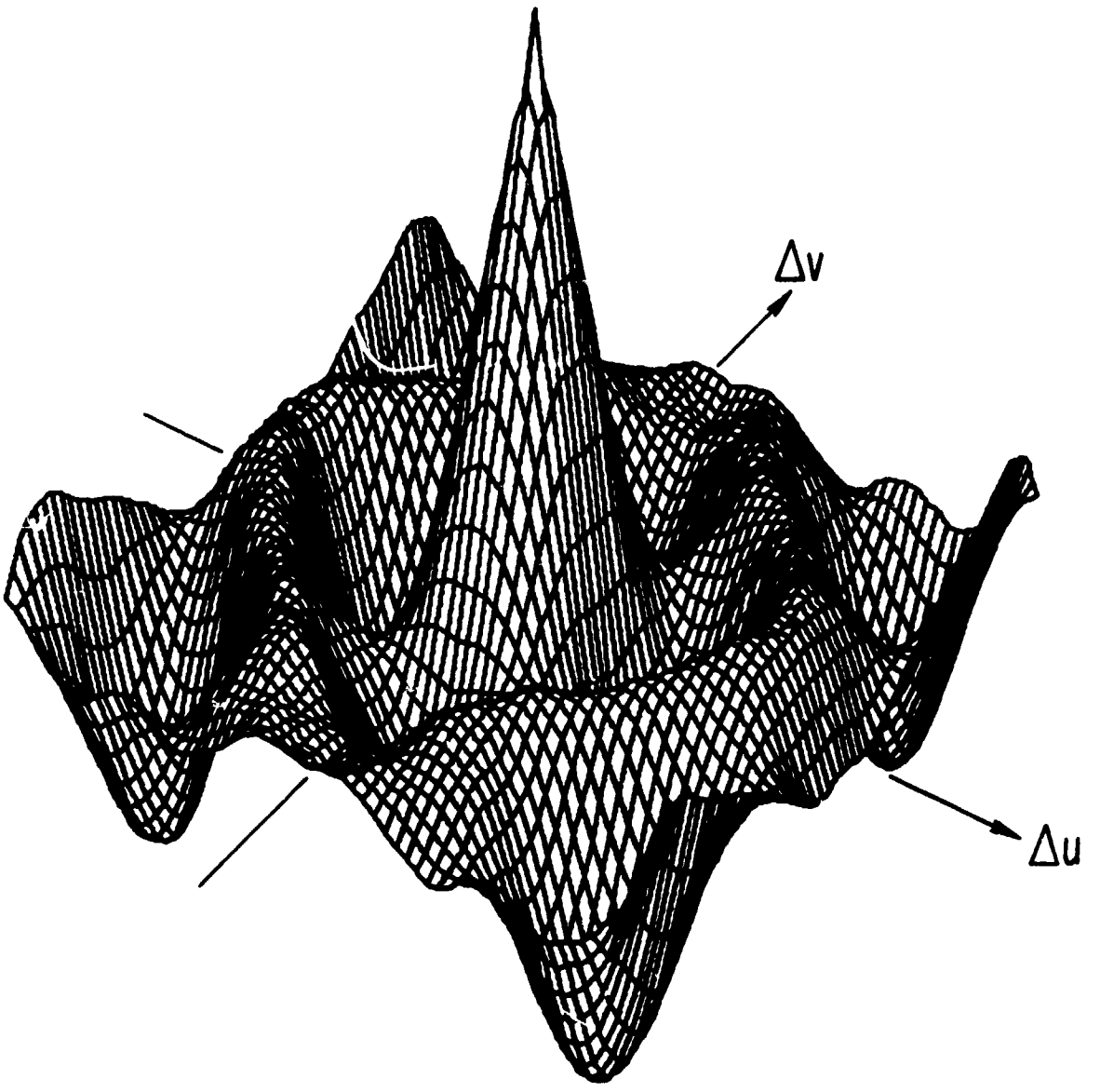

Fig. 12 Perspective View of the Sine Alpha Autocorrelation Function in the Presence of Collimation

Thus far the number of bits carried in the beam steering computation is large so that truncation errors are not significant. Figures 13 and 14 illustrate the importance of row and column truncation errors. Figure 13 shows the effect of truncating row and column steering commands to 6 bits. The rms error is increased noticeably to 0.228 ms. In Fig. 14, the row and column steering commands have been truncated to 4 bits, and this results in a situation where the row and column truncation errors dominate the phase shifter truncation errors, even though 4 bits are employed in the adder and only 3 bits in the phase shifter. The rms error for this case is 0.45 ms. This computational result has been corroborated with an approximate theoretical analysis.

Note that the antisymmetry property of ϵ_u is preserved. Furthermore, it has been observed that the error ϵ_u in the present case with 4-bit row and column truncation is almost periodic, with a period which is half the period given by the 3-bit phase shifter. The error is not exactly periodic at the half-period intervals because of the presence of the error due to the 3-bit phase shifter.

C. Effect of Randomized Quantization Levels

As discussed in Sec. II-D, quantization level randomization is an effective technique for eliminating spatially correlated phase errors which give rise to quantization lobes, i.e., large angle errors, in certain directions. Figure 15 illustrates the error obtained in the absence of space feed collimation but with quantization levels randomized. Note the absence of any symmetry. As expected, the rms error is very close to the theoretically predicted value of 0.149 ms. The autocorrelation function width is not materially different, however, when compared to the autocorrelation functions of the previous cases. Figure 16 shows $\epsilon_u(u, v)$ in the same scanning sector as Figs. 8 and 11. Some of the regular features discernible in Fig. 11 are absent in the present case. The ϵ_v surface has a generally similar character. Figure 17 shows the autocorrelation function $R_u(\Delta u, \Delta v)$. $R_v(\Delta u, \Delta v)$ has a similar shape. The shape of these surfaces near the central peak is very similar to that

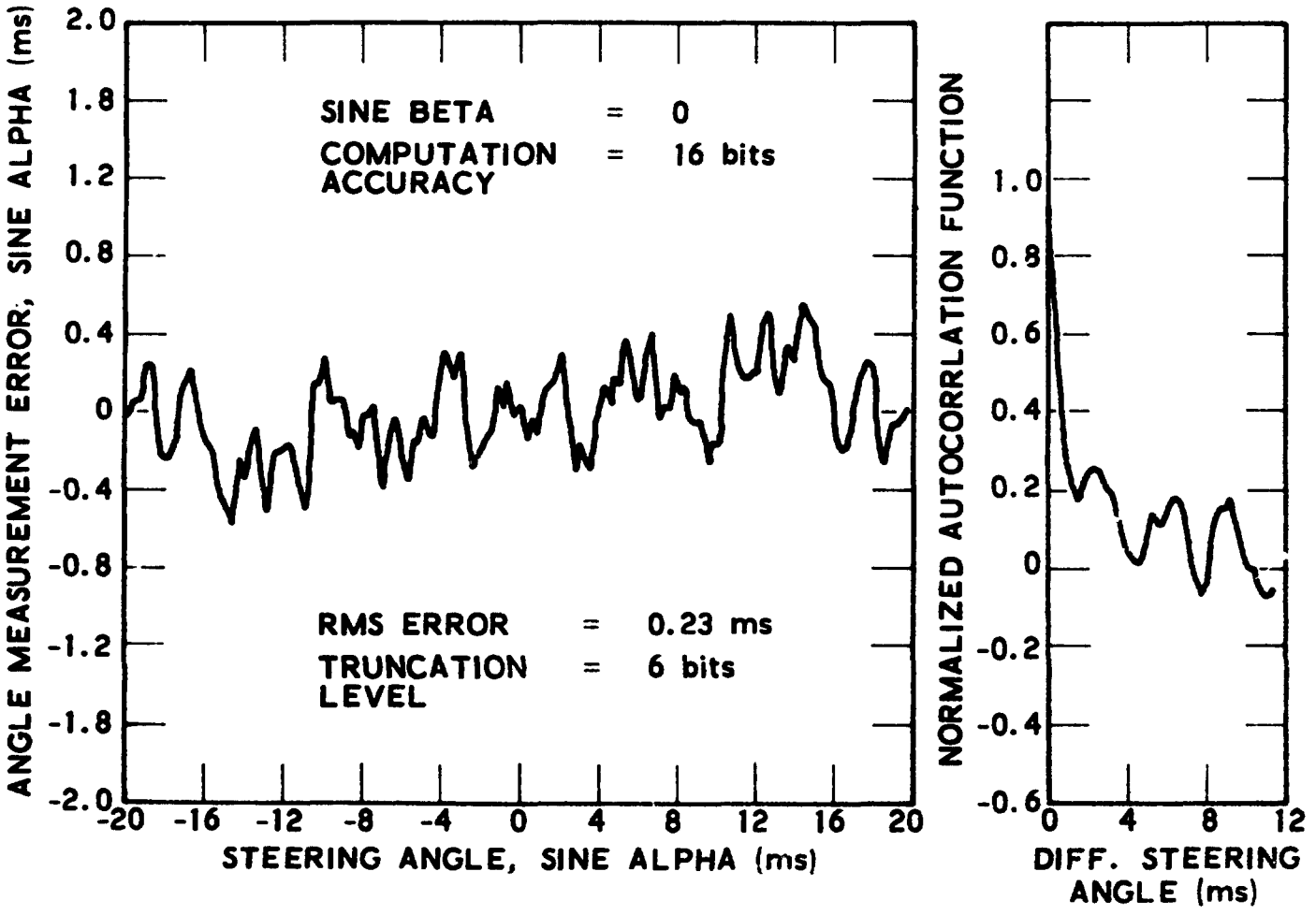

Fig. 13 Sine Alpha Error with Intermediate Adder Bit Level in the Presence of Collimation

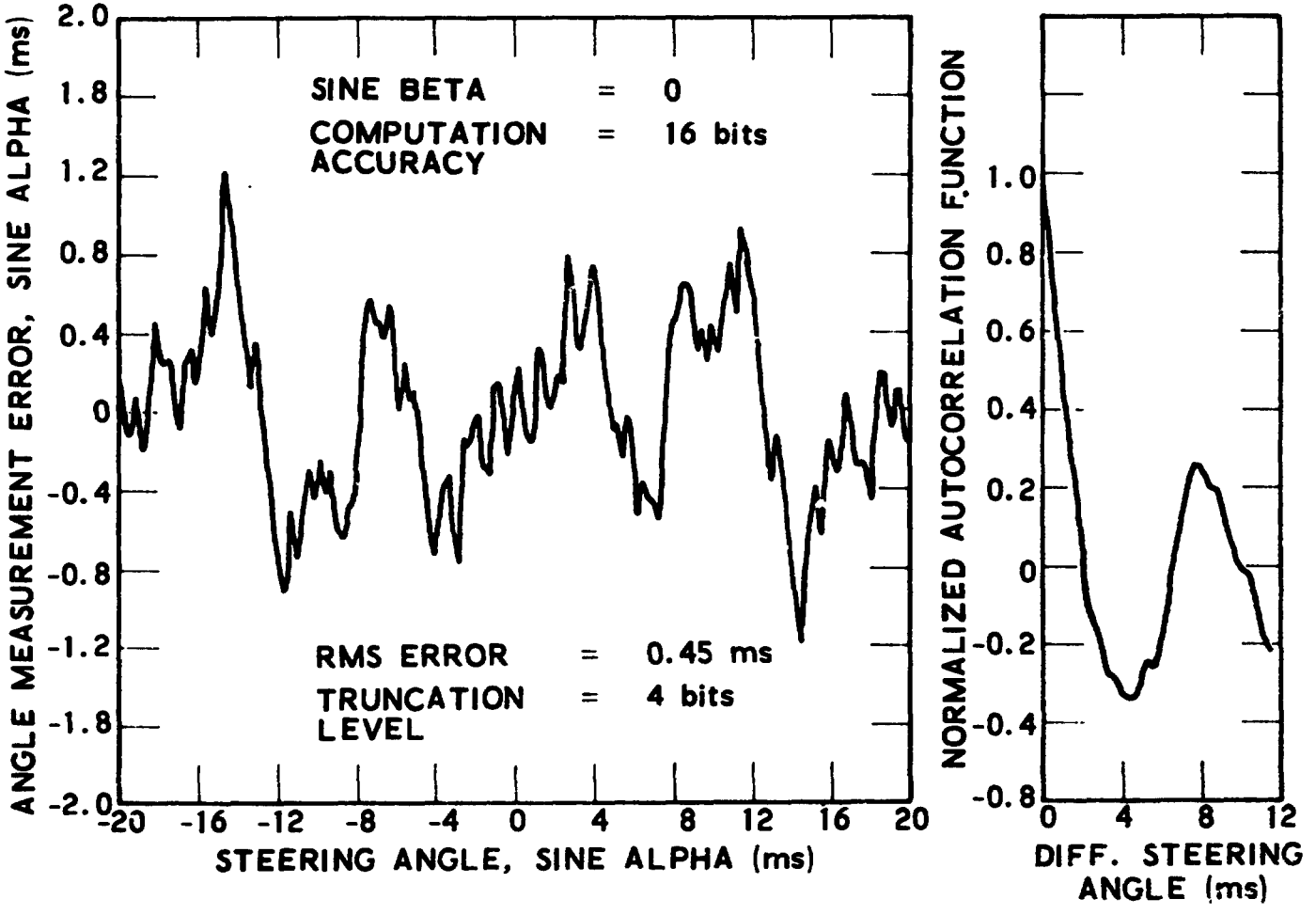

Fig. 14 Sine Alpha Error with Low Adder Bit Level in the Presence of Collimation

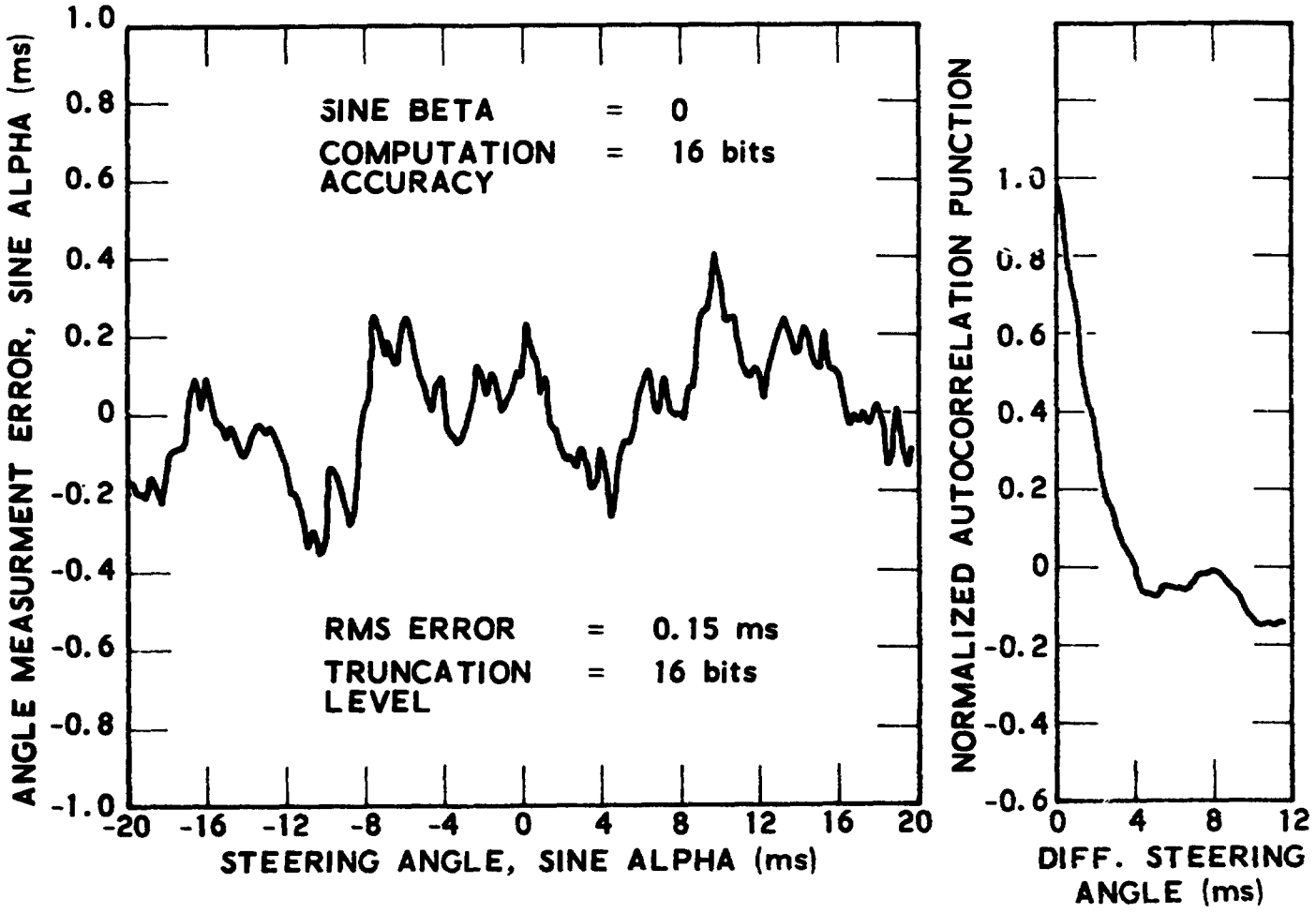

Fig. 15 Sine Alpha Error in the Presence of Randomized Quantization Levels

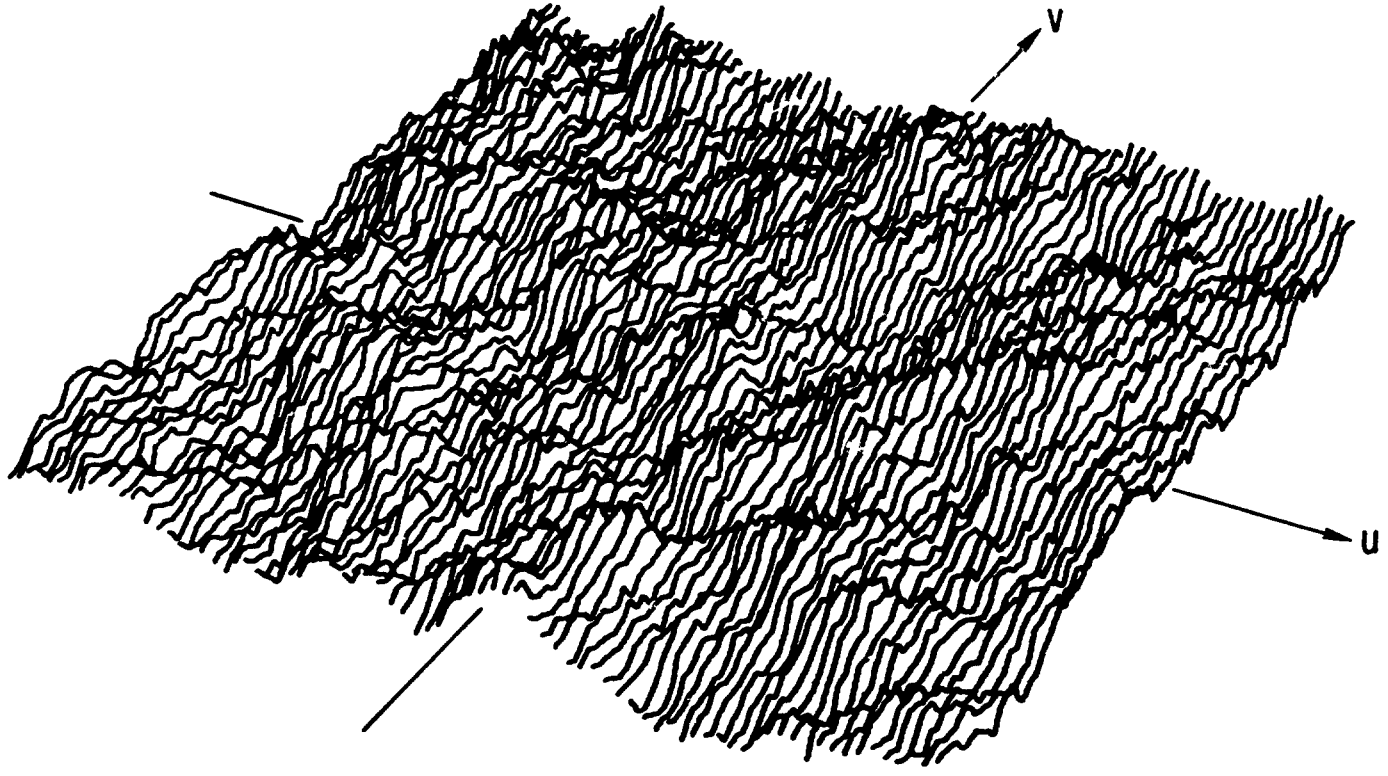

Fig. 16 Perspective View of the Sine Alpha Error in the Presence of Randomized Quantization Levels

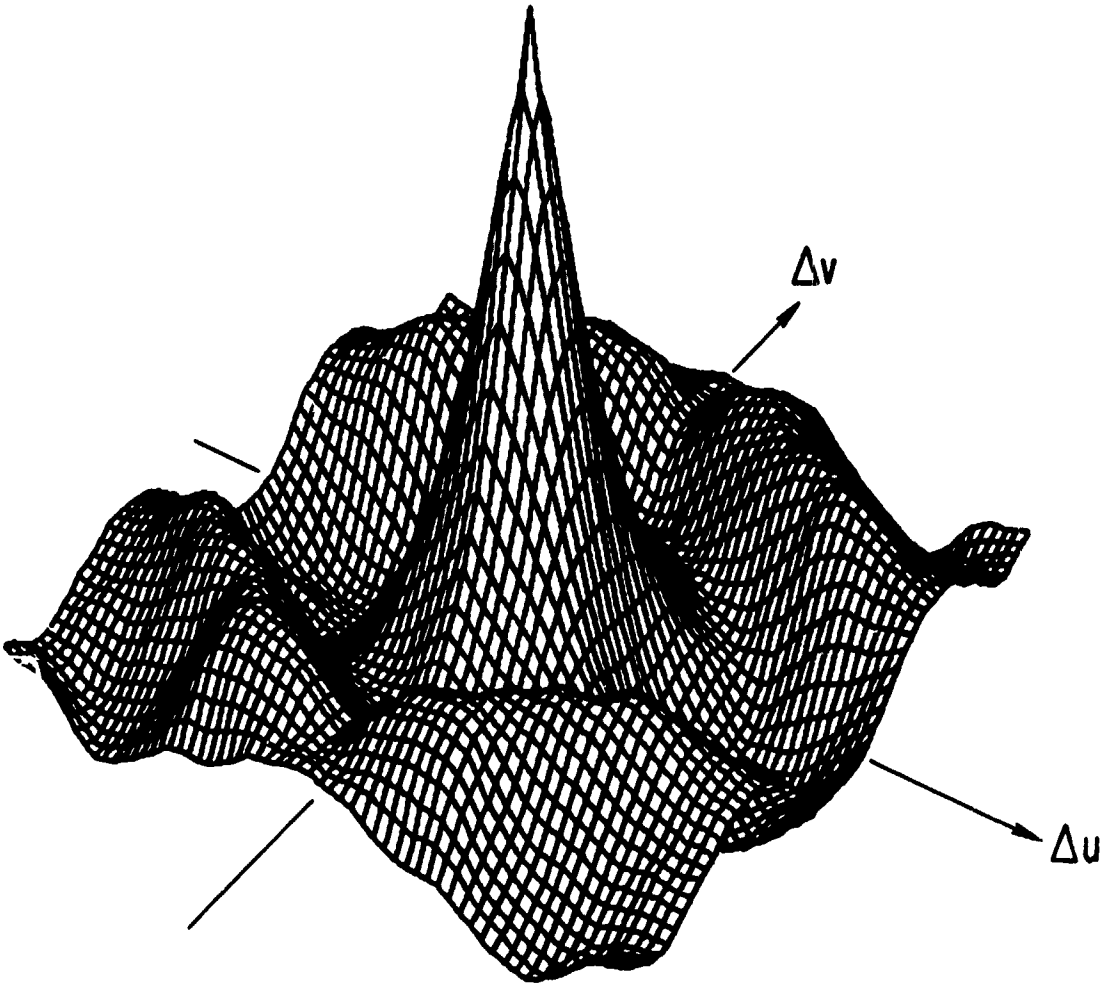

Fig. 17 Perspective View of the Sine Alpha Autocorrelation Function in the Presence of Randomized Quantization Levels

shown in Fig. 12 for the space feed collimation case. This result indicates that the spatial statistics of the angular error in the case of randomized quantization levels is generally similar to the case where space feed collimation is employed. The width of the central peak at the 3 dB point is still about 2 ms, as it is in those cases employing collimation.

D. Differential Phase Errors

Thus far differential phase errors have been ignored. Figure 18 illustrates the effects of including moderately large differential phase errors in an array with randomized quantization levels. In this configuration a 10°, one-sigma random differential phase error is generated for each bit with the aid of a gaussian random number generator and stored for later use by the computer program. The errors so generated are independent from bit to bit, even within the same phase shifter element. The increase in the rms error shown in Fig. 18 is representative of the large sector average increase in rms error due to 10°, one-sigma differential phase errors. To compare the relative magnitude of these differential phase errors to the quantization error for the case of 3-bit phase shifters, consider the total differential phase error ζ_{mn} at element mn:

$$\zeta_{mn} = \epsilon_1\gamma_1 + \epsilon_2\gamma_2 + \epsilon_3\gamma_3$$

where

ϵ_i = ith bit differential phase error, i = 1, 2, 3

γ_i = ith bit state function, i = 1, 2, 3

$$= \begin{cases} 1 \text{ if bit i is "on"} \\ 0 \text{ if bit i is "off"} \end{cases} .$$

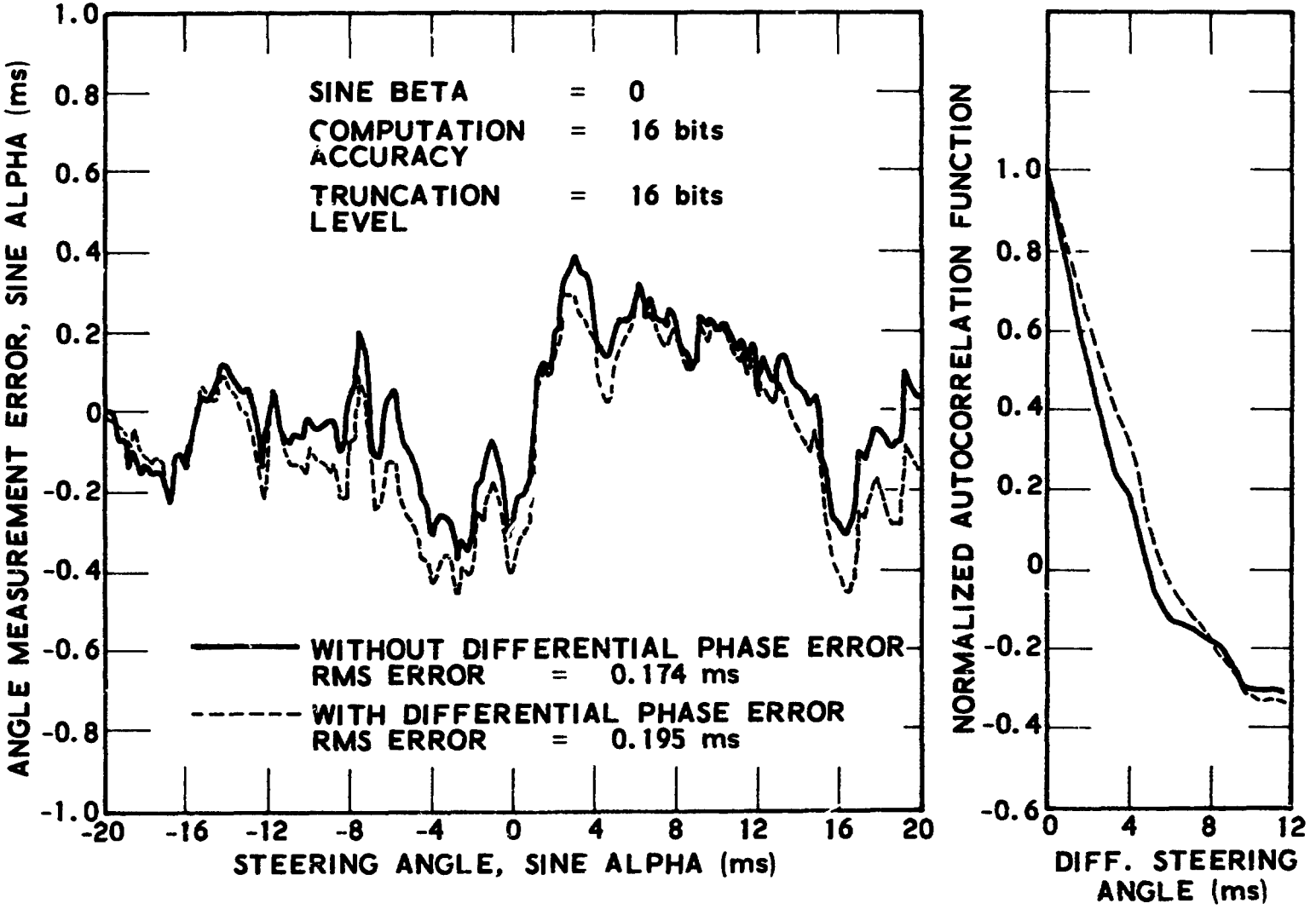

Fig. 18 Sine Alpha Error with Randomized Quantization Levels and 10° Differential Phase Errors

The subscript mn has been omitted from ϵ_i and γ_i for brevity. By appropriate averaging over the states of γ_i, and ensemble averaging over the states of ϵ_i, it is readily shown that

$$\overline{\sigma_\zeta^2} = \frac{1}{4}\left(\sigma_{\epsilon_1}^2 + \sigma_{\epsilon_2}^2 + \sigma_{\epsilon_3}^2\right) \quad .$$

With $\sigma_{\epsilon_1} = \sigma_{\epsilon_2} = \sigma_{\epsilon_3} = 10°$, the rms differential phase error, denoted σ_ζ, is given by

$$\sigma_\zeta = 8.67° \quad .$$

The error ξ_{mn} (in the absence of differential phase errors) is uniformly distributed over the interval $\pm Q/2$ ($= \pm 22.5°$). Therefore, for $q = 3$ and $\epsilon_i = 0$,

$$\sigma_\xi = 13.0° \quad .$$

The inclusion of the differential phase error of 8.67° causes the error σ_ξ to increase from 13.0 to 15.6°. This increase affects σ_u and σ_v proportionately, as shown by Eqs. (9) and (10).

Since the differential phase errors can be made significantly less than 10° rms, these results provide good justification for ignoring differential phase errors as an important source of angular measurement error. It is for this reason that differential phase errors have been ignored in the other cases presented.

A plot similar to Fig. 18 for the case of space feed collimation shows that the presence of differential phase errors destroys the symmetry and periodicity properties noted earlier. To the extent that the differential phase errors are small, these symmetry and periodicity properties are approximately obeyed.

V. DECORRELATION TECHNIQUES AND COMPUTATIONAL RESULTS

If the pulse-to-pulse correlations in the angle measurement error prove to be of consequence, it may be desirable to implement one of several dithering techniques to reduce these correlations. The principal techniques for accomplishing decorrelation are (a) phase dithering, (b) frequency dithering, and (c) beam dithering. These techniques produce decorrelation of the angle errors by forcing random fluctuation of the element phase commands from look to look.

The angle correlation is due to phase error (ξ_{mn}) correlation from look to look. The purpose of the dithering techniques, therefore, is to generate commands that will tend to make the element phase error uncorrelated from look to look. Typically, the element phase error need only change by a phase of $Q/4$ ($Q = 2\pi/2^q$) to effect nearly complete decorrelation.

A. Phase Dithering

The phase dithering technique consists of generating a random phase angle (from 0 to 2π) and adding it to each phase shifter phase command. This is most easily done in the beam steering computer, where the randomly generated angle can be added to each row or column command. The resultant change in the absolute phase of the wave front leaves the direction of the beam unchanged and is of no consequence for many applications. In general, the only situation of interest in which the random phase could be undesirable is the case of second time around returns (or higher order range ambiguities) from clutter, if phase coherent clutter rejection techniques are required.

Figure 19 shows the sine alpha error surface ϵ_u in the same scan sector as the previous perspective plots. In this case, however, phase dithering has been added to the ordinary row and column collimation

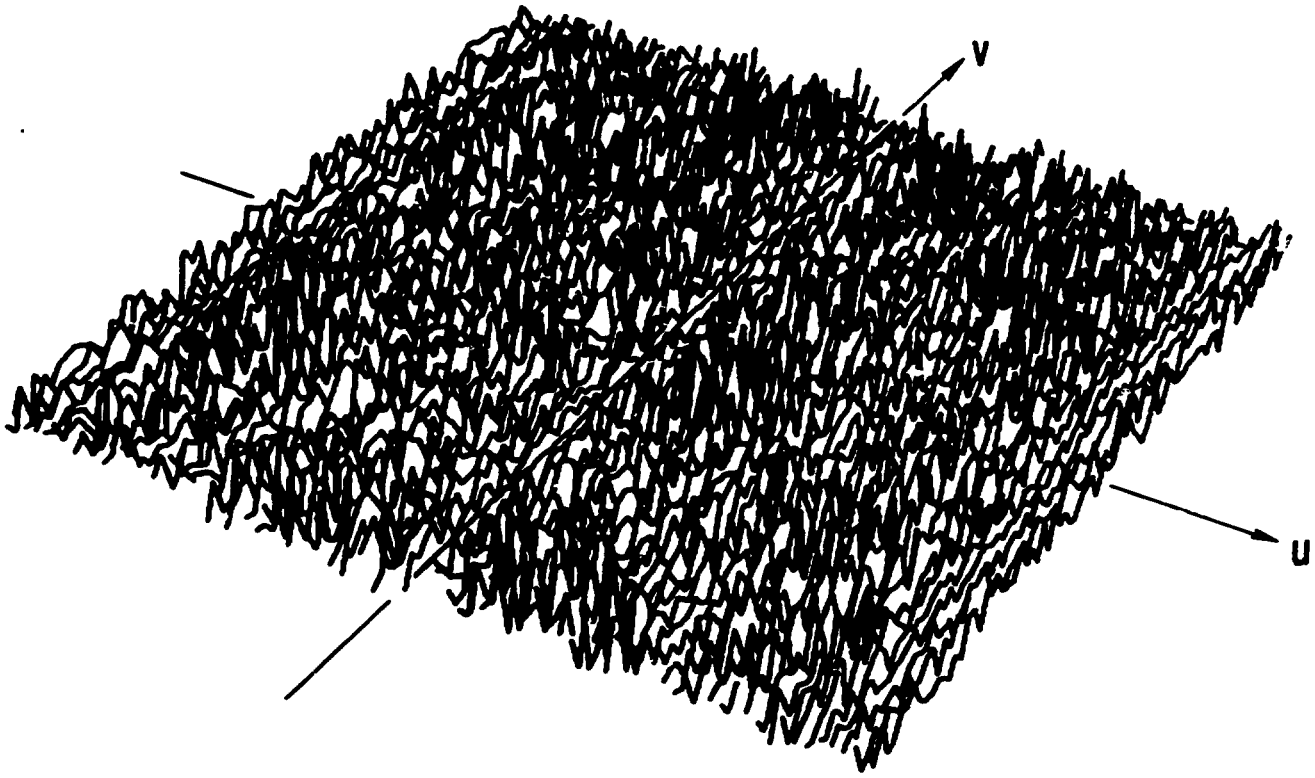

Fig. 19 Perspective View of the Sine Alpha Error Surface with Collimation and Phase Dithering

configuration whose results were presented in Sec. IV-B. While this error surface appears to be much "hashier" than the surface of Fig. 11, the really dramatic change in the correlation properties can best be seen in the subsequent plot of $R_u(\Delta u, \Delta v)$ in Fig. 20. The behavior of $R_v(\Delta u, \Delta v)$ is identical to $R_u(\Delta u, \Delta v)$. The error decorrelates completely in a differential angle equal to the spacing between looks, in this case, 0.5 ms. Actually, it is not necessary to move the beam at all to obtain decorrelation with phase dithering.

The time-domain autocorrelation function of the measurement error, with or without beam motion, contains an identically large central peak with complete decorrelation in a time equivalent to the inter-pulse period, i.e., the rate at which the phase shifters are dithered. This technique is equally effective in space-fed and corporate-fed arrays.

B. Frequency Dithering

The essential array design requirement for effective decorrelation through frequency dithering is that the phase shifter phase command include an angle which compensates for the feed-to-phase shifter propagation delay. Thus, if the frequency is changed, the compensation phase changes, resulting in a new phase error. All space-fed planar arrays fall into this category. A corporate fed structure with varying cable lengths to each array element could also be designed to employ frequency dithering.

Frequency dithering, while not as easy to implement as phase dithering, is a technique which will often be available for other reasons. In particular, frequency agility is sometime implemented for ECCM or increased detection range against scintillating targets. In these cases, instrument error decorrelation is an additional benefit to consider. Frequency dithering has the disadvantage of destroying pulse-to-pulse phase coherence which might be desirable for coherent integration and/or clutter rejection.

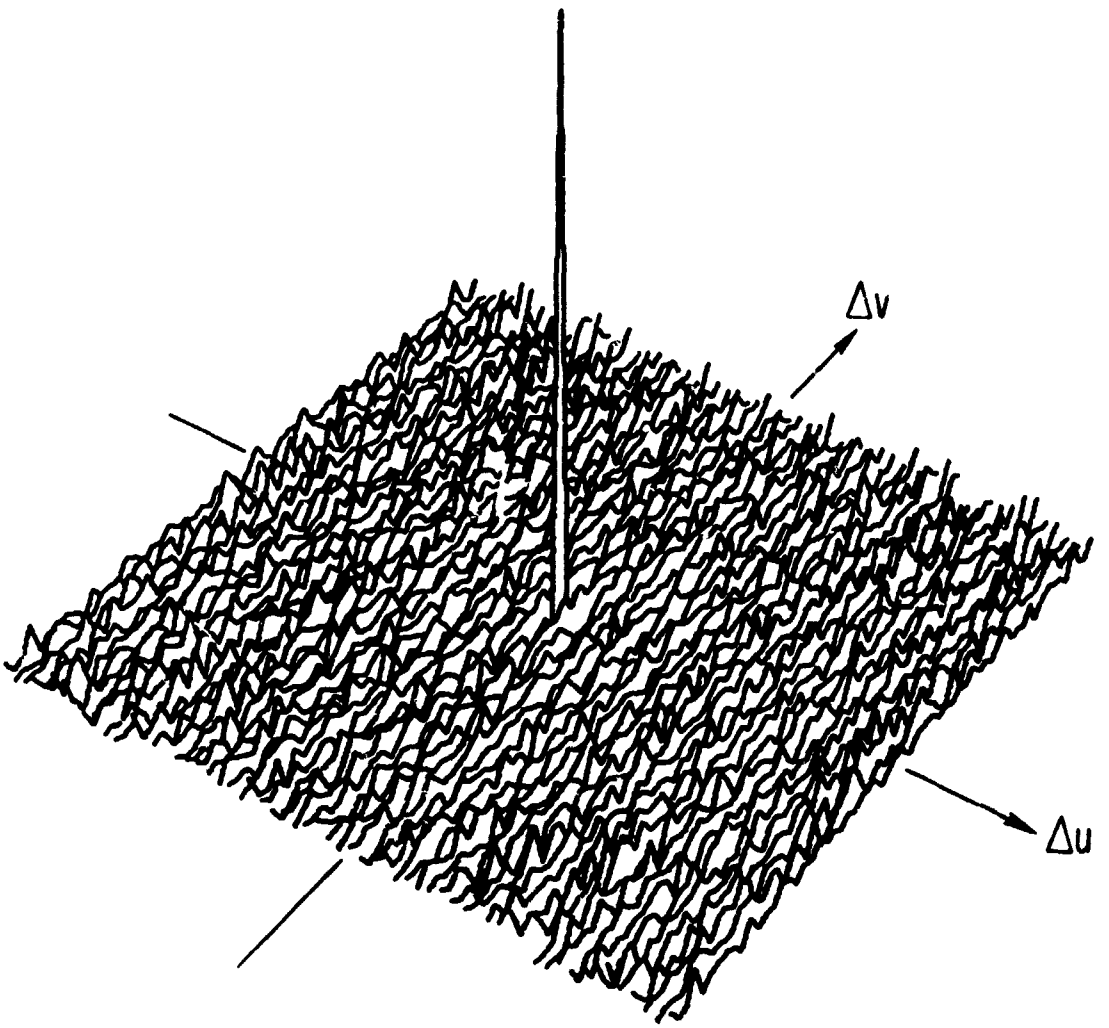

Fig. 20 Perspective View of the Sine Alpha Autocorrelation Function with Collimation and Phase Dithering

Figure 21 shows that frequency dithering is equally effective in decorrelating the error. This space-fed configuration was scanned over the same sector as Fig. 11. The total range of frequency dither in this case is 10% (±5%), uniformly distributed across the band. On each radar look, a new operating frequency within the band is chosen on a random basis. It is easy to show that a 5% change in frequency causes most of the phase shifters to change by at least Q/4.

C. Beam Dithering

The angle errors, as shown in Sec. IV-B, indicate that correlations for the particular array studied never exceeded more than a few millisines. A natural decorrelation technique, therefore, is to steer the beam slightly more than necessary, in a random way, so as to enhance the natural decorrelation that already exists. The resulting degradation due to off-axis tracking is small, since the total excursion due to dithering can be chosen to be much less than a beamwidth. The implementation of this technique is also quite simple. It is entirely contained in the beam steering computer. A random number generator selects two angles within specified limits. These are then simply added to the beam steering computer input steering commands.

In order to generate an error surface which has the correlation properties shown in Fig. 22, a random angle generator was used which produced variates with a uniform distribution from -5 ms to +5 ms, or about 20% of the beamwidth. The beam is dithered to a new random angle (both u and v) on each radar look. The correlation function is seen to drop very rapidly to a small pedestal and then becomes very small. This technique might be improved by changing the distribution of the randomly varying angle commands, although this possibility has not been investigated. A disadvantage of beam dithering is that the total beam excursion is limited somewhat by off-axis degradation. In situations where MTI is employed to reject clutter, beam dithering may seriously degrade MTI performance. It is concluded that beam dithering is a good decorrelation technique but is less attractive than frequency dithering.

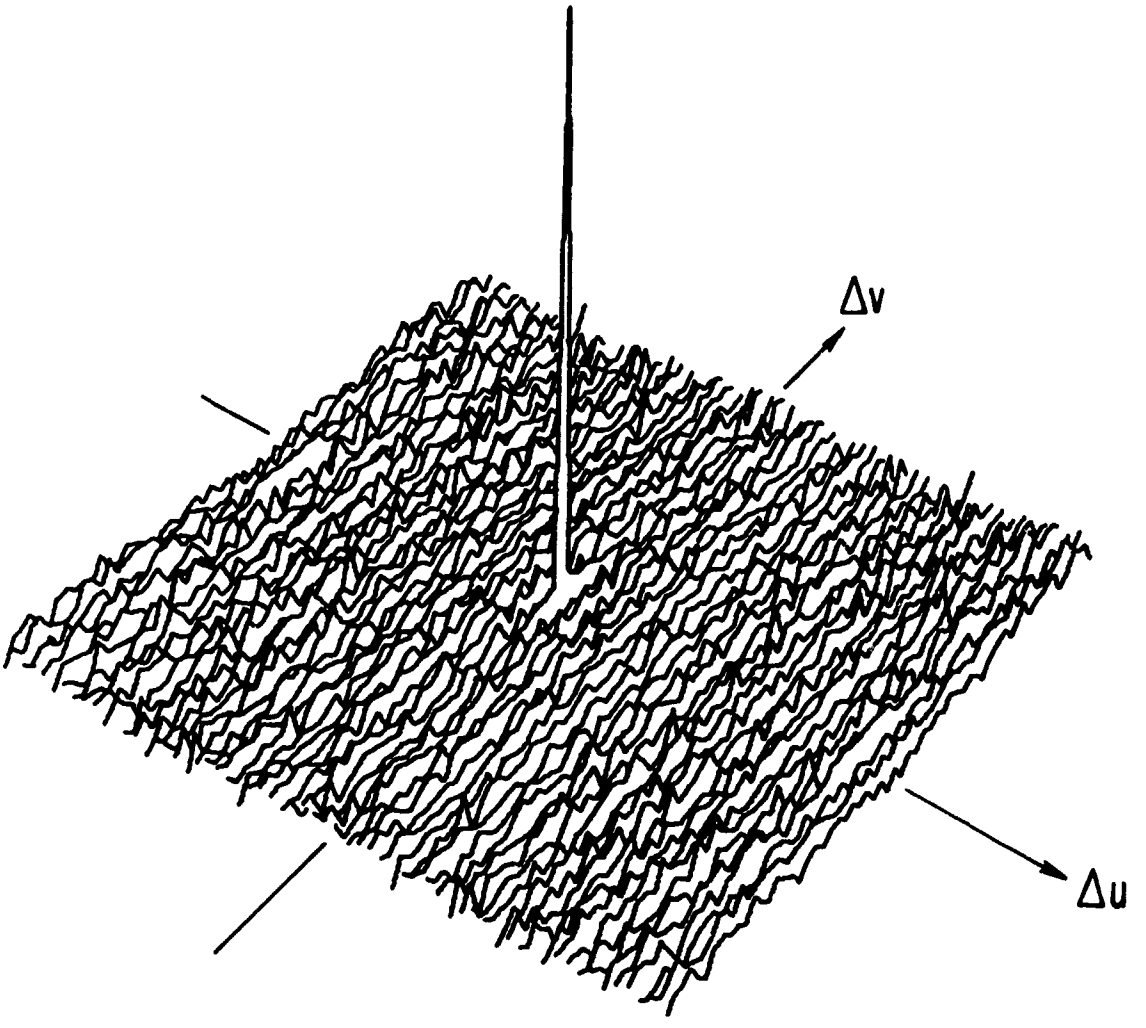

Fig. 21 Perspective View of the Sine Alpha Autocorrelation Function with Collimation and Frequency Dithering

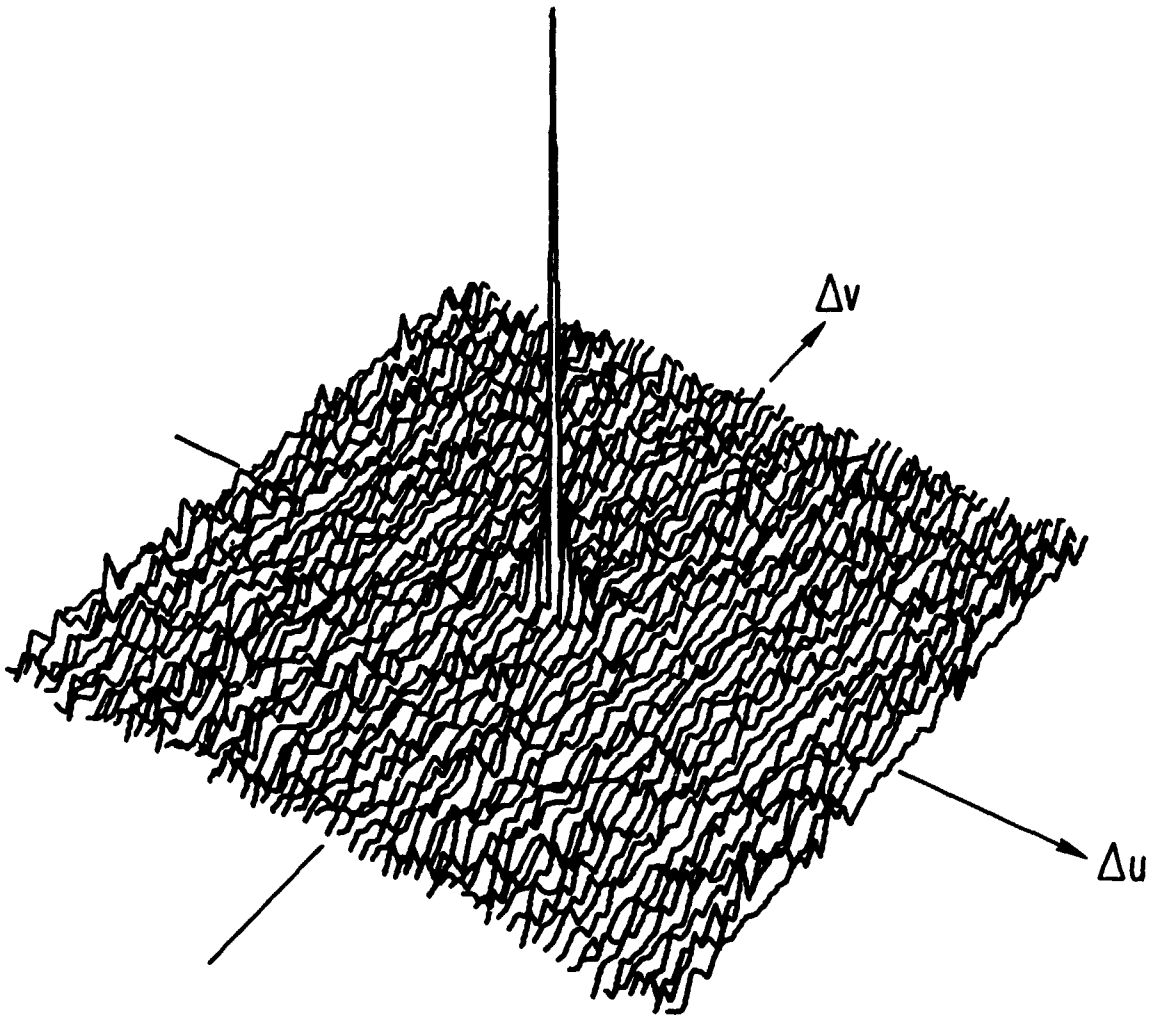

Fig. 22 Perspective View of the Sine Alpha Autocorrelation Function with Collimation and Beam Dithering

VI. SUMMARY

This paper describes an analysis of the random instrumentation angle measurement errors of phased array radars. A number of calculations of angle measurement errors were performed for a particular, though typical, array configuration. These calculations were aided by a comprehensive computer program, which was developed in sufficiently general form to permit its application to a wide class of phased array radars. The program simulates finite computation accuracy in the beam steering computer, truncation of steering commands at the row and column level, truncation of steering commands at the phase shifters, and the effects of differential phase errors. The example array was examined in various modes of operation, with and without quantization level randomization and with and without space-feed collimation. The effects of row and column adder computation accuracy were examined. The statistical behavior of the angle measurement error with and without several dithering techniques was determined. For the typical array configuration considered, the following conclusions can be drawn:

a. A beam split ratio (neglecting bias errors) in excess of 300:1 can be achieved with the use of only 3-bit phase shifters.

b. Truncation of row and column steering commands was found to dominate the angle error in certain array configurations. In these cases the beam split ratio may be reduced below 100:1 and the angle error is nearly periodic at a submultiple of the array period.

c. Differential phase errors as large as 10°, one-sigma per bit were found to have only a minor effect on rms angular measurement error. The rms error increased only about 20%. A bias error on the order of 0.1 ms was also observed.

d. A steering angle of approximately 2 ms in any direction will cause a 50% drop in the autocorrelation of the angular errors.

The horizontal cross section of the central peak of the two-dimensional autocorrelation function is roughly circular, i.e., there are not strong "preferred" correlation directions.

e. The phase dithering technique was shown to be completely effective in annihilating all angle measurement error correlations. Results were presented for a typical sector scan, but beam steering is not necessary. This technique is very easy to implement.

f. Frequency dithering was also shown to be an effective decorrelation technique. Beam dithering was found to be somewhat less effective than frequency or phase dithering. Both frequency and beam dithering involve compromises which may make them unacceptable for certain applications.

APPENDIX A
RMS ERROR FOR VARIOUS APERTURE WEIGHTING FUNCTIONS

The Eqs. (9) and (10) show that the rms angle measurement error is dependent on the difference pattern amplitude weighting functions δ_x and δ_y. It is the purpose of this appendix to show that the rms error is only weakly dependent on the actual shape of the difference pattern. It is intuitively obvious that those weighting functions that tend to place more weight on the phase shifters at the edges of the array will tend to produce lower rms angle errors. On the other hand, such functions tend to produce larger sidelobes. To illustrate the effects of various difference pattern weighting functions on the rms error, Eqs. (9) and (10) were numerically evaluated on a small programmable desk calculator (HP9100A). The results are compared in Table A-1.

Only the x-difference pattern weighting function is illustrated in Table A-1. Note that this is assumed to be independent of y. The y-difference pattern weighting function was assumed to be the same as the x-difference pattern with the variable y replacing x. To summarize,

$$\delta_x(x, y) = \delta_x(x)$$

$$\delta_y(x, y) = \delta_y(y) = \delta_x(y) \quad .$$

Other applicable parameters are as defined in Sec. IV. The results in Table A-1 show that the rms error spread is likely to be less than 25% of a representative mean value for all those weighting functions of practical interest.

Table A-1 RMS Angle Measurement Error for Various Amplitude Weighting Functions

WEIGHTING FUNCTION		ONE-SIGMA ERROR
SINE	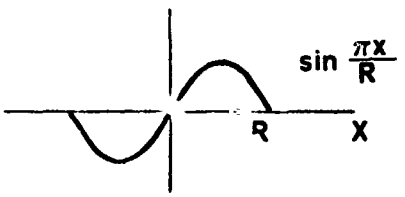	σ_u = 0.1486 ms σ_v = 0.1485 ms
LINEAR	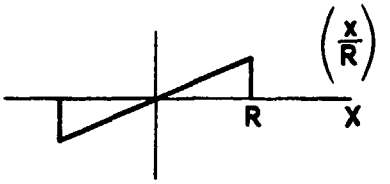	σ_u = 0.1258 ms σ_v = 0.12[illegible]3 ms
CUBIC	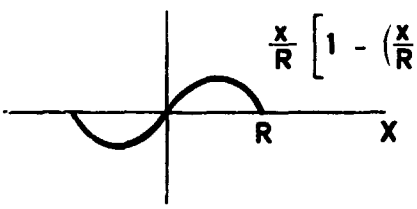	σ_u = 0.1406 ms σ_v = 0.1404 ms
TRUNCATED RAYLEIGH	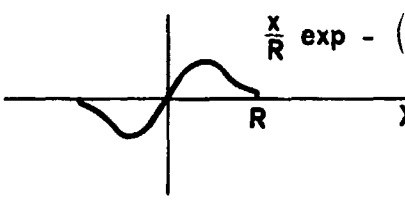	σ_u = 0.1775 ms σ_v = 0.1775 ms
UNIFORM	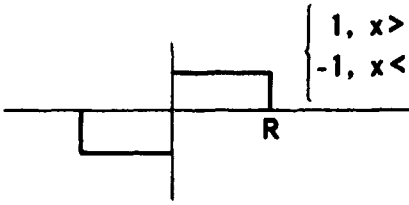	σ_u = 0.1464 ms σ_v = 0.1482 ms

REFERENCES

1. D. Barton, Handbook of Radar Measurements, McGraw-Hill, 1969.

2. W. J. Albersheim, "Reduction of Side Lobes and Pointing Errors in Phased Array Radars by Randomizing Quantization Steps," Report No. TM-3435, The Mitre Corp., AD 402953, Apr. 1963.

3. D. R. Rhodes, Introduction to Monopulse, McGraw-Hill, 1959.

4. W. H. Nester, "A Study of Tracking Accuracy in Monopulse Phased Arrays," IRE Transactions on Antennas and Propagation, p. 237, May 1962.

5. B. R. Hatcher, "Collimation of Row-and-Column Steered Phased Arrays," Proc. IEEE, p. 1787, Nov. 1968.